nucl-th/9705041

INTERPLAY OF PARTON AND HADRON CASCADES IN NUCLEUS-NUCLEUS COLLISIONS AT THE *CERN SPS* AND *RHIC*

Klaus Geiger and Ronald Longacre

Physics Department, Brookhaven National Laboratory, Upton, N.Y. 11973, U.S.A.

e-mail: klaus@bnl.gov, longacre@bnl.gov

Abstract

We introduce a Monte Carlo space-time model for high-energy collisions with nuclei, involving the dynamical interplay of perturbative QCD parton production and evolution, with non-perturbative parton-cluster formation and 'afterburner' cascading of formed pre-hadronic clusters plus hadron excitations. This approach allows us to trace the space-time history of parton and hadron degrees of freedom of nuclear collisions on the microscopical level of parton and hadron cascades in both position and momentum space, from the instant of nuclear overlap to the final yield of particles. In applying this approach, we analyze $Pb + Pb$ collisions at the CERN SPS with beam energy 158 GeV ($\sqrt{s}/A = 17$ GeV) and Au+Au collisions at RHIC with collider energy $\sqrt{s}/A = 200$ GeV. We find that the perturbative QCD parton production and cascade development provides an important contribution to particle production at central rapidities, and that the 'afterburner' cascading of pre-hadronic clusters and formed hadrons emerging from the parton cascade is essential. The overall agreement of our model calculations including the 'afterburner' cascading with the observed particle spectra at the CERN SPS is fairly good, whereas the neglect of the final-state interactions among hadronic excitations deviates significantly.

I. INTRODUCTION

The physics of QCD at high density has become in the last years a most important field of research, for example, in the context of the rise of the gluon structure functions in deeply inelastic ep scattering at very small x [1], the propagation of hard probes in dense nuclear matter such as jets [2] or charmonium [3], or, the issue of formation and evolution of a quark-gluon plasma in collisions of heavy nuclei [4]. Hence, high-density QCD effects are notoriously present, in one way or another, in high-energy collision experiments that involve interactions of hadronic or nuclear matter, hence offering a diverse resort of exciting new physics.

Specifically the experimental heavy-ion programs at the CERN SPS (currently under way), the RHIC and LHC colliders (to be launched in the next few years), are concepted in the hope of discovering novel collective behavior of highly compressed nuclear matter through characteristic particle production from this dense matter. In this scope, the prime motivation for ultra-relativistic heavy-ion collisions is to create a state of high particle- and energy-density, and to study the decay of the system to gain knowledge of QCD interactions under these extreme conditions. The characteristics of particle production in the environment of dense, strongly interacting matter should teach us about significance and properties of the interplay between partonic and hadronic degrees of freedom, i.e., fundamental questions concerning deconfinement dynamics, formation and evolution of a quark-gluon plasma, the nature of the QCD phase-transition between quark-gluon and hadron phases, et cetera.

Clearly, to extract unambigous signatures of these new physics aspects from 'messy' nuclear collision events with several hundreds, or even thousands of final-state particles, a good understanding of the microscopic dynamics is required, that is, the evolution from the initial state of colliding nuclei, via parton and hadron production, up to the final appearance of particles in the detectors. Here lies the essential concern of this paper, namely, to study the role and relative importance of partons and hadrons, as well as their dynamical interplay, in a generally mixed parton-hadron system created by a high-energy collision of two heavy nuclei. To do so, we take steps towards a phenomenological, QCD-based, description that combines quark-gluon *and* hadron degrees of freedom in the evolution of nucleus-nucleus collisions at CERN SPS energies and above.

To the best of our knowledge no constructive attempt has been made before to merge the perturbative QCD parton-cascade picture with a hadron-cascade model. On the contrary, the event generators that are currently on the market for desribing nucleus-nucleus collisions are exclusivily based on modelling nuclear collisions in terms of nucleon-nucleon collisions on the basis of a constituent valence-quark picture plus string-excitation and -fragmentation. Popular examples for these models are FRITIOF [5], VENUS [6], RQMD [7], DPM [8]. Distinct from these is HIJING [9], which also incorporates a perturbative QCD approach to multiple minijet production, however, it does not incorporate a space-time description. In particular VENUS and RQMD are impressively fine-tuned to describe the recent CERN SPS data. Yet, the price paid is the invention of supplemental mechansims (such as 'string droplets' in VENUS or 'color ropes' in RQMD) to mimic certain underlying dynamics due to nuclear effects, which cannot be accounted for in non-trivial manner.

Our rationale is different: We strictly refrain from introducing ad-hoc recipes to parametrize physics details that may be novel in nuclear collisions as compared to hadronic collisions. Rather, we wish to examine in how far a well-defined semiclassical multi-particle description in terms of partons and hadrons suffices to accomodate the bulk characteristics of the CERN data, and hence may serve as a prospect for RHIC and LHC heavy-ion physics. We will not address here the fundamental nature of complex underlying physics aspects; instead we adopt a probabilistic particle description with dynamically changing proportions of partons and hadrons, and develop a space-time model that allows to simulate nucleus collisions from the first instant of overlap, via QCD parton cascade development at the early stage, parton conversion into pre-hadronic excitations and hadron formations, up to the cascading of these pre-hadrons and final state particles, as well as the beam remnant nucleons at late times. As we shall show, this approach does remarkably well in comparison to the gross particle production properties observed at CERN SPS. No attempt is made to fine-tune our model to the data, and hence we presume that a more detailed analysis than carried out in this paper, may exhibit disagreement, in which case this may be taken as indicator of truly new physics.

To set the stage, we recall the standard picture of high-energy hadron collisions as compared to hadron-nucleus or nucleus-nucleus collisions (for convenience we view the collisions in the overall center-of-mass frame):

- In *hadron-hadron collisions* with large momentum transfer, the coherence of the incoming hadron wavefunctions is (at least partially) destroyed upon collisional contact by means of one or more hard parton scatterings and/or by soft non-diffractive interactions between the beam hadrons. The liberated partons that materialize mostly around midrapidity after a hard scattering, evolve as jets (accompanied by gluon radiation), and eventually reorganize to color-singlet systems that form final state hadrons around central rapidities $|y| \approx y_{cent} \equiv 0$. On the other hand, the remnants of the initial hadrons that have not taken part in the hard process, recede down the beam pipe with little energy loss, and produce hadron fragments around $|y| \lesssim |y_{beam}|$, near the beam rapidities $y_{beam} = \pm \ln(\sqrt{s}/M_h)$. The dynamics of parton evolution and hadron production at small rapidities should therefore decouple to good approximation from the fragmentation of the beam remnants at large rapidities. As is well known, such a behaviour is indeed observed at $p\bar{p}$ collider experiments with $\sqrt{s} \gtrsim 100$ GeV, in which the measured baryon rapidity distributions shows two seperate peaks around $\pm y \approx y_{beam}$ with a distinct gap in between, whereas the rapidity distributions of mesons is strongly concentrated in the central region. This characteristic behaviour of hadron-hadron collisions is usually termed *transparency*.

- In *nucleus-nucleus collisions* at beam energies per nucleon comparable to proton-proton colliders, the picture of a fairly clean separation of the three rapidity regions (central, forward and backward beam fragmentation regions) as in hadron collisions breaks down. Nonetheless, the basic dynamics of particle production parallels those in hadronic collisions, except that it is amplified by the large interaction volume of the nuclear collision system. Hence, much larger number of hard parton scatterings is likely to be initiated by sufficiently large momentum transfer collisions of nucleon pairs from the two beam nuclei, leading to copious parton materialization and (mini)jet production in the central rapidity region. The beam remnants containing the spectator nucleons on the other hand populate the forward and backward rapidity regions, but to lesser extent than in hadronic collisions at comparable energy. However, it is a well known experimental fact that in nucleus-nucleus collisions a rigid division into the three rapidity regions is not possible anymore. Rather than transparency, one observes a significant *stopping* associated with slowing down of the initial nucleons due to inelastic nucleon-nucleon collisions, on top of the nucleons energy loss from hard parton production. Moreover, there are effects of *rescattering* among partons, among initial state nucleons, as well as among newly produced final state hadrons. Rescattering consequently must lead to an enhanced particle production and $p_\perp$-broadening in the central region, whereas stopping causes a significant baryon population at midrapidity as well as a smearing of the peaks at forward and backward beam rapidities.

The preceding qualitative discussion serves us as motivation for investigating the space-time dynamics of nucleus-nucleus collisions within a combined parton-hadron cascade model, raising the following two key questions:

1. To which extent undergo the colliding nuclei materialization of partonic constituents, what is the relative importance of associated parton cascading, and how does the simultanous evolution of co-existing partonic and hadronic matter proceed in space and time?

2. What is the cumulate effect on final-state particle distributions from the space-time history of rescatterings among partons during the early stage, and from re-interactions involving the remnant nucleons as well as newly formed hadronic excitations at later times?

The paper is organized as follows. In Sec. II, we introduce in brevity some formal aspects of multi-particle kinetic theory, which form the theoretical basis of our QCD space-time cascade model. Sec. III is devoted to the application of the model to heavy-ion coollisions, first to $Pb + Pb$ collsions at CERN SPS energy of $\sqrt{s}/A = 17$ GeV, and then to $Au + Au$ collsions at RHIC energy of $\sqrt{s}/A = 200$ GeV. Sec. IV contains concluding remarks and discusses some future perspectives.

II. DESCRIPTION OF THE MODEL

In this Section we explain the main aspects of our parton-hadron cascade model. We will not be concerned here with the elaborate details of the model, but refer the interested reader to the extensive documentations of Refs. [10,11] for the parton cascade aspects and Refs. [12] for the hadron cascade features. The central element in our space-time cascade description is the use of relativistic transport theory [11] in conjunction with renormalization-group improved QCD [13], which provides the theoretical basis to follow the QCD evolution in 7-dimensional phase-space d^3rd^3kdE of a mixed multi-particle system of partons and hadrons with dynamically changing proportions.

As we explain further below, we combine the following four elements: (i) the *initial state* of the nucleus-nucleus collision system in terms of ncleon and parton degrees of freedom, (ii)the *parton-cascade development* which embodies the perturbative QCD evolution of multiple parton collisions including inelastic (radiative) processes, (iii) the phenomenological *parton-hadron conversion* model of Ellis and Geiger [14–16], in which the hadronization mechanism is described in terms of dynamical parton-cluster formation with subsequent decay of color-singlet clusters into hadrons, and, (iv) the *'afterburner' hadron cascade* of produced pre-hadronic clusters and hadrons which incorporates cluster-cluster, cluster-hadron, hadron-hadron collisions, as well as resonance formation and decay.

The microscopic history of the dynamically-evolving particle system is traced in space-time *and* momentum space, so that the correlations of particles in space, time, color and flavor can be taken into account systematically. We emphasize that the interplay between perturbative and non-perturbative regimes is controlled locally by the space-time evolution of the mixed parton-cluster-hadron system itself (i.e., the time-dependent local particle densities), rather than by an arbitrary global division between parton and hadron degrees of freedom (i.e., a parametric energy/momentum cut-off). In particular the parallel evolution of the mixed system of partons, pre-hadronic clusters, and hadrons, with the relative proportions determined by the dynamics itself, is a novel feature that is only possible by keeping track of both space-time and energy-momentum variables.

The model as a whole consists of four major building-blocks, describing the above-mentioned evolution stages of a nucleus-nucleus collision from the initial beam/target collision system upon collisional contact, through the QCD-evolution of parton distributions, hadron formation and cascading, up to the emergence of final hadronic states:

(i) The *initial state* associated with the incoming nuclei involves their decomposition into nucleons and of the nucleons into partons on the basis of the experimentally measured nucleon structure functions and elastic form-factors. This procedure translates the initial nucleus-nucleus system into two colliding clouds of *virtual* partons according to the well-established parton decpomposition of the nuclear wavefunctions at high energy [17].

(ii) The *parton cascade development* starts from the initial interpenetrating parton clouds, and involving the space-time development with mutual- and self-interactions of the system of quarks and gluons. Included are multiple elastic and inelastic interaction processes, described as sequences of elementary $2 \to 2$ scatterings, $1 \to 2$ emissions and $2 \to 1$ fusions. Moreover, correlations are accounted for between primary virtual partons, emerging as unscathed remainders from the initial state, and secondary real partons, materialized or produced through the partonic interactions.

(iii) The *hadronization dynamics* of the evolving system in terms of parton-coalescence to color-neutral clusters is decribed as a local, statistical process that depends on the spatial separation and color of nearest-neighbor partons. Each pre-hadronic parton-cluster fragments through isotropic two-body decay into primary hadrons, according to the density of states, followed by the decay of the latter into final stable hadrons.

(iv) The *'afterburner' hadron cascade* describes the evolution of produced pre-hadronic clusters and hadrons, emerging both from the hadronization of cascading partons, as well as from primary remnant partons which represent the fraction of unscathed initial state nucleons. Pre-hadronic clusters can mutually rescatter, or scatter off close-by hadrons, before they decay into stable final-state hadrons. Similarly, already formed hadrons may deflected by elestic collisions with other hadrons and clusters, or may be excited by inelastic collisions and resonance formation/decay.

A firm theoretical basis for the above space-time cascade description of a multiparticle system in high-energy collisions can be derived systematically from *quantum-kinetic theory* on the basis of QCD's first principles in a stepwise approximation scheme (see e.g., Refs. [13,18] and references therein). This framework allows to cast the time evolution of the mixed system of individual partons, composite parton-clusters, and physical hadrons in terms of a closed set of integro-differential equations for the phase-space densities of the different particle excitations. The definition of these phase-space densities, denoted by F_α, where $\alpha \equiv p, c, h$ labels the species of partons, pre-hadronic clusters, or hadrons, respectively, is:

$$F_\alpha(r,k) \;\equiv\; F_\alpha(t,\vec{r};E,\vec{k}) \;=\; \frac{dN_\alpha(t)}{d^3r d^3k dE}\;, \tag{1}$$

where $k^2 = E^2 - \vec{k}^{\,2}$ can be off-shell (space-like $k^2 < m^2$, time-like $k^2 > m^2$) or on-shell ($k^2 = m^2$). The densities (1) measure the number of particles of type α at time t with position in $\vec{r} + d\vec{r}$, momentum in $\vec{k} + d\vec{k}$, and energy in $E + dE$ (or equivalently invariant mass in $k^2 + dk^2$). The F_α are the quantum analogues of the classical phase-space distributions, including both off-shell and on-shell particles, and hence contain the essential microscopic information required for a statistical description of the time evolution of a many-particle system in complete 7-dimensional phase-space $d^3r d^3k dE$, thereby providing the basis for calculating macroscopic observables.

The phase-space densities (1) are determined by the self-consistent solutions of a set of *transport equations* (in space-time) coupled with renormalization-group type *evolution equations* (in momentum space). Referring to Refs. [14,13] for details, these equations can be generically expressed as convolutions of the densities F_α of particle species α, interacting with specific cross sections $\hat{I}_j$ for the processes j. The resulting coupled equations for the space-time development of the densities of partons F_p, clusters F_c and hadrons F_h is a self-consistent set in which the change of the densities F_α is governed by the balance of the various possible interaction processes among the particles. As compared to Ref. [10], here we consider in novel addition the 'afterburner' cascade of clusters and hadrons as mentioned before. Figs. 1-3 represents these equations pictorially. For the densities of partons F_p, the *transport equation* (governing the space-time change with r^μ) and the *evolution equation* (controlling the change with momentum scale k^μ), read, respectively, (Fig. 1),

$$\begin{aligned} k_\mu \frac{\partial}{\partial r^\mu}\, F_p(r,k) = {} & F_{p''}F_{p'''} \circ \Big[\, \hat{I}(p''p''' \to pp') \;+\; \hat{I}(p''p''' \to p) \Big] \;-\; F_p F_{p'} \circ \Big[\, \hat{I}(pp' \to p''p''') \;+\; \hat{I}(pp' \to p'') \Big] \\ & -\; F_p F_{p'} \circ \Big[\, \hat{I}(p'p'' \to p) \;-\; \hat{I}(pp' \to p'') \Big] \;-\; F_p\, F_{p'} \circ \hat{I}(pp' \to c) \end{aligned} \tag{2}$$

$$k^2 \frac{\partial}{\partial k^2}\, F_p(r,k) = F_{p'} \circ \hat{I}(p' \to pp'') \;-\; F_p \circ \hat{I}(p \to p'p'')\;. \tag{3}$$

For the densities of *pre-hadronic clusters* and *hadrons*, the evolution equations are homogeneous to good approximation, so that one is left with non-trivial transport equations only, *. For the evolution of the cluster densities F_c, we have (Fig. 2)

---

* It is worth noting that eq. (3) embodies the momentum space (k^2) evolution of partons through the renormalization of

$$k_\mu \frac{\partial}{\partial r^\mu} F_c(r,k) = F_p\, F_{p'} \circ \hat{I}(pp' \to c) \;-\; F_c \circ \hat{I}(c \to h) \;+\; F_{c''} F_{c'''} \circ \hat{I}(c''c''' \to cc') \;-\; F_c F_{c'} \circ \hat{I}(cc' \to c''c''') \tag{4}$$
$$+\, F_{c'} F_{h'} \circ \hat{I}(c'h' \to ch) \;-\; F_c F_h \circ \hat{I}(ch \to c'h') \;+\; \ldots\ldots$$
$$k^2 \frac{\partial}{\partial k^2} F_c(r,k) = 0\,, \tag{5}$$

and similarly, for the evolution of the hadron densities F_h, the equations read (Fig. 3)

$$k_\mu \frac{\partial}{\partial r^\mu} F_h(r,k) = F_c \circ \hat{I}(c \to h) \;+\; \Big[\, F_{h'} \circ \hat{I}(h' \to h) \;-\; F_h \circ \hat{I}(h \to h') \Big] \;+\; F_{h''} F_{h'''} \circ \hat{I}(h''h''' \to hh') \tag{6}$$
$$-\, F_h F_{h'} \circ \hat{I}(hh' \to h''h''') \;+\; F_{c'} F_{h'} \circ \hat{I}(c'h' \to ch) \;-\; F_c F_h \circ \hat{I}(ch \to c'h') \;+\; \ldots\ldots$$
$$k^2 \frac{\partial}{\partial k^2} F_h(r,k) = 0\,. \tag{7}$$

In (2)-(7), each convolution $F \circ \hat{I}$ of the density of particles F entering a particular vertex $\hat{I}$ includes a sum over contributing subprocesses, and a phase-space integration weighted with the associated subprocess probability distribution of the squared amplitude. Explicit expressions are given in Refs. [11,14].

The terms on the right-hand side of the transport- and evolution-equations (2)-(7) corresponds to one of the following categories (c.f. Figs. 1-3):

- parton scattering and parton fusion through 2-body collisions,
- parton multiplication through radiative emission processes on the perturbative level,
- colorless cluster formation through parton coalescence depending on the local color and spatial configuration,
- hadron formation by decay of the cluster excitations into final-state hadrons.
- scattering of pre-hadronic clusters or already formed hadrons with other clusters or hadrons. Note: this includes also (as indicated by the 'dots') cluster-cluster fusion, cluster-hadron absorption, as well as inelastic collisions among clusters and hadrons, in which energy-momentum is transferred into excitation.

The equations (2)-(7) reflect a *probabilistic interpretation* of the multi-particle evolution in space-time and momentum space in terms of sequentially-ordered interaction processes j, in which the rate of change of the particle distributions F_α ($\alpha = p, c, h$) in a phase-space element $d^3r d^4k$ is governed by the balance of gain (+) and loss (−) terms. The left-hand side describes free propagation of a quantum of species α, whereas on the right-hand side the interaction kernels $\hat{I}$ are integral operators that incorporate the effects of the particles' self- and mutual interactions. This probabilistic character is essentially an effect of time dilation, because in any frame where the particles move close to the speed of light, the associated wave-packets are highly localized to short space-time extent, so that comparatively long-distance quantum interference effects are generally small.

---

the phase-space densities F_p, determined by their change $k^2 \partial F_p(r,k)/\partial k^2$ with respect to a variation of the mass (virtuality) scale k^2 in the usual QCD evolution framework [19–21]. On the other hand, for pre-hadronic clusters and hadrons, renormalization effects are comparatively small, so that their mass fluctuations $\Delta k^2/k^2$ can be ignored to first approximation, implying $k^2 \partial F_c(r,k)/\partial k^2 = k^2 \partial F_h(r,k)/\partial k^2 = 0$.

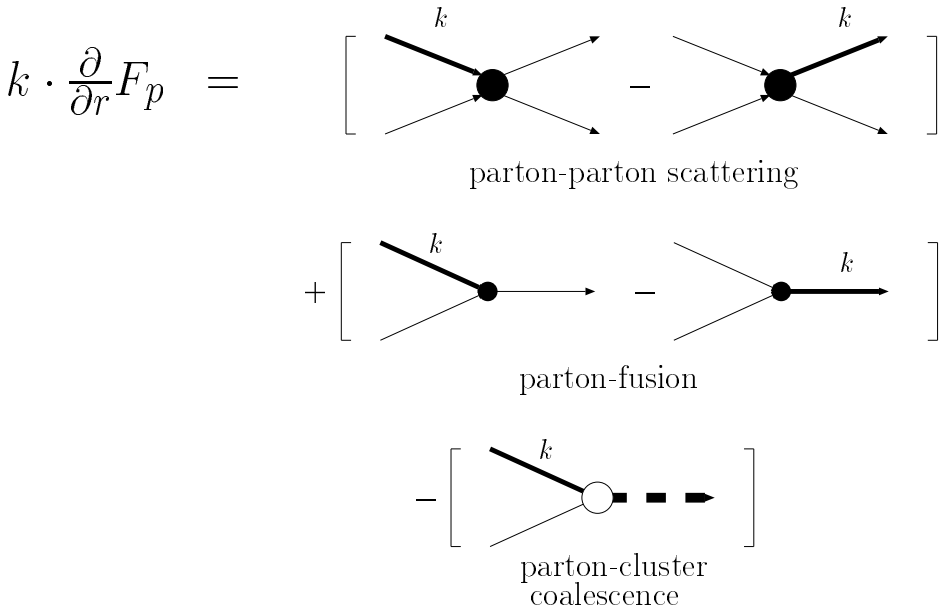

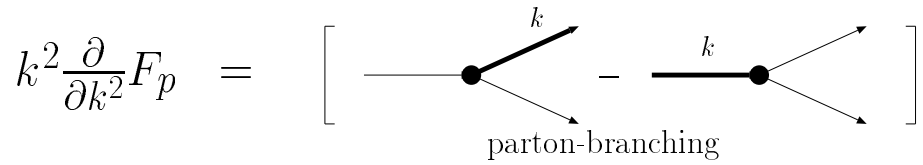

FIG. 1. Graphical representation of the equations (2) and (3) for the particle phase-space densities F_p of partons.

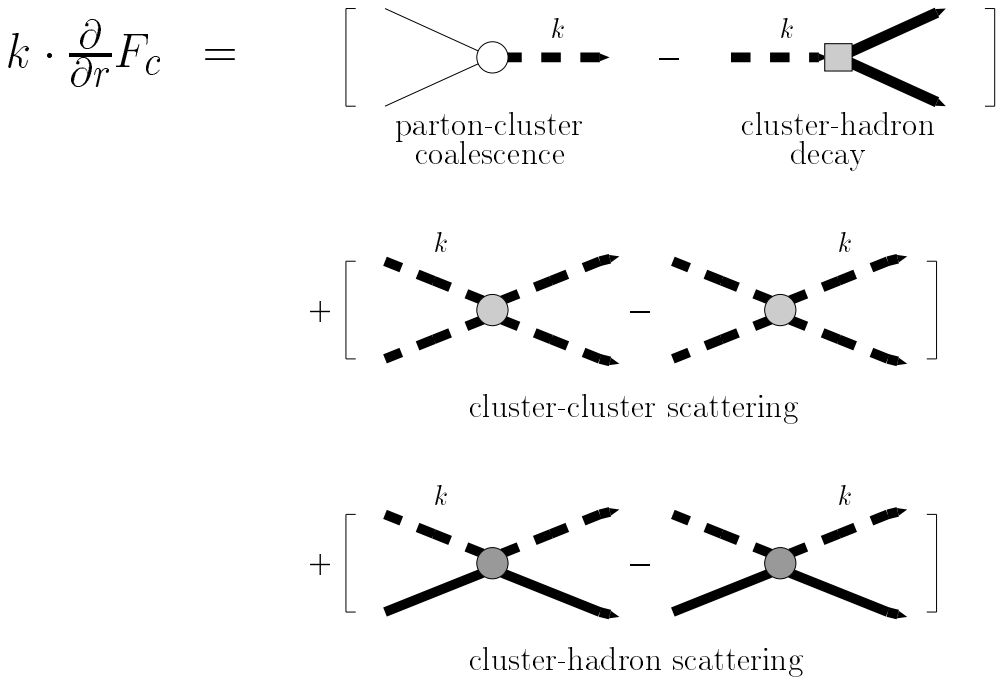

$$k^2 \frac{\partial}{\partial k^2} F_c \;\approx\; 0$$

FIG. 2. Graphical representation of the equations (4) and (5) for the particle phase-space densities F_c of pre-hadronic clusters. The 'dots' represent further processes not explicitely shown, such as cluster-cluster fusion, cluster-hadron absorption, as well as inelastic collisions among clusters and hadrons, in which energy-momentum is transferred into excitation.

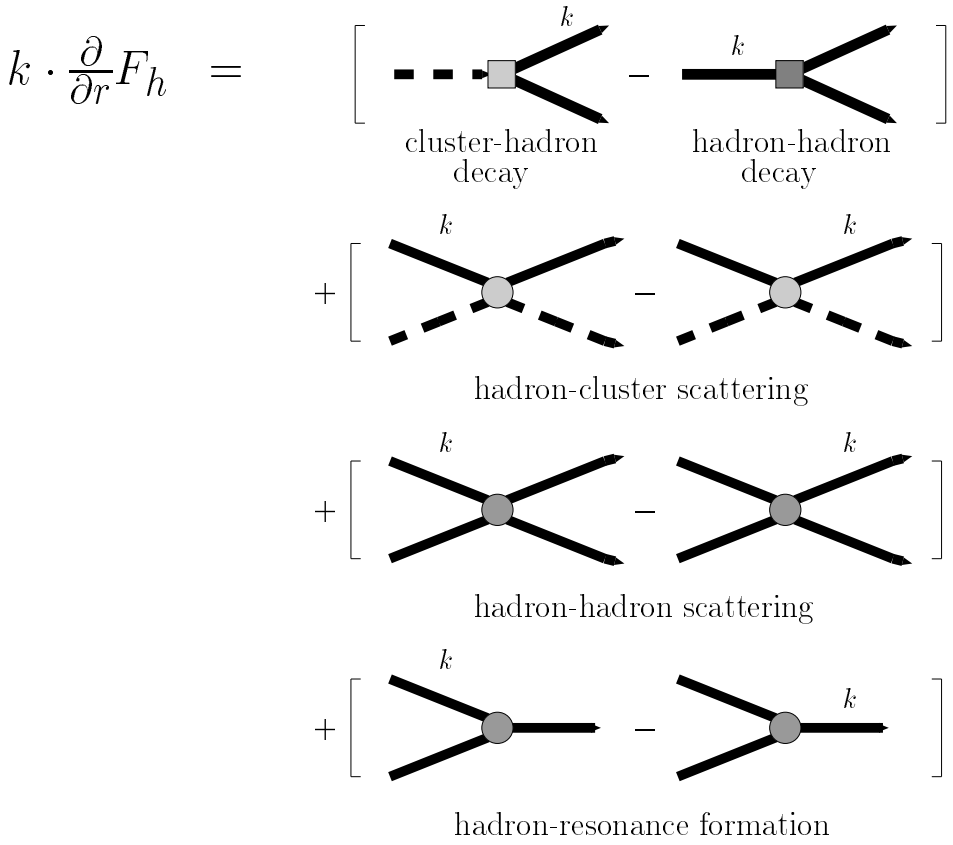

$$k^2 \frac{\partial}{\partial k^2} F_h \approx 0$$

FIG. 3. Graphical representation of the equations (6) and (7) for the particle phase-space densities F_h of hadrons. The 'dots' represent further processes not explicitely shown, such as cluster-hadron absorption, as well as inelastic collisions among clusters and hadrons.

III. APPLICATION TO HEAVY-ION COLLISIONS AT THE *CERN SPS* AND *RHIC*

In this Section we apply the our approach to heavy-ion collisions, first, to $Pb+Pb$ collisions at the nominal CERN SPS beam energy 158 GeV, corresponding to a center-of-mass energy per nucleon of $\sqrt{s}/A = 17$ GeV, and second, to $Au+Au$ collisions at the anticipated RHIC energy per nucleon of $\sqrt{s}/A = 200$ GeV. We restict ourselves to these collision systems, because $Pb+Pb$ at the CERN SPS is the largest nuclear system at the highest present energy that has actually been studied in experiment with the recent data from the '96 and '97 runs hinting first evidence of new physics apsects in high-energy nuclear collisions, and because $Au+Au$ at RHIC is the comparable collision system at an order of magnitude larger beam energy. However, we emphasize that our model applys in general to any collision system $A+B$ including proton-nucleus collisions at energies $\sqrt{s}/A \gtrsim 10$ GeV. In particular, we believe its strength lies in addressing nuclear collisions at even higher energies, such as anticipated at the LHC.

In applying our model in practice, we note that the probabilistic character of the transport- and evolution equations (2)-(7) allows one to solve for the phase-space densities $F_\alpha(r,k)$ by simulating the dynamical development as a Markovian process causally in time. The computer simulations, the details and results of which we will discuss below, were performed by combining the parton- cascade/cluster-hadronization code VNI [10] the hadron cascade code HIJET [12]. Starting from the initial parton clouds $F_p(t_0,\vec{r},k)$, corresponding to the incoming nuclei upon collisional contact at time $t=t_0$, the set of equations (2)-(7) can be solved in terms of the evolution of the phase-space densities F_p, F_c and F_h of partons, clusters, and hadrons, respectively, for $t > t_0$. For calculational convenience, it is most suitable to choose the *center-of-mass (cm) frame of the colliding beam particles*, with the collision axis in the z-direction. We remark that in general the space-time description of particle evolution is Lorentz-frame dependent, however, since we are concerned in the following only with Lorentz-invariant final-state hadron spectra in rapidity and transverse mass, the particular choice of frame is irrelevant for the results and just a matter of preference.

A. The simulation procedure

The simulation of the time development of the mixed system of partons, clusters, and hadrons in position and momentum space on the basis of eqs. (2)-(7) emerges then from following each individual particle through its history with the various probabilities and time scales of interactions sampled stochastically from the relevant probability distributions in the kernels $\hat{I}$ of eqs. (2)-(7): The microspcopic history of the system can thus be traced by evolving the phase-space distributions of particles are evolved in small time steps ($\Delta t \simeq 10^{-3}\ fm$) and 7-dimesional phase-space d^3rd^3kdE throughout the stages of parton cascade, parton-cluster formation, cluster-hadron decays, and afterburner hadron cascade, until stable final-state hadrons and other particles (photons, leptons, etc.) are left as freely-streaming particles. The essential ingredients in this Monte-Carlo procedure are summarized as follows [10]:

(i) The *initial state* is constructed in three steps. First, the nuclei are decomposed into the nucleons with an appropriate Fermi-distribution. Second, the nucleons are in turn decomposed into their parton substructure according to proton/neutron structure functions [†] with a spatial distribution given by the Fourier transform of the nucleon elastic form-factor. Third, the so-initialized phase-space densities of (off-shell) partons are then boosted with the proper Lorentz factor to the center-of-mass frame of the colliding nuclei.

(ii) The *parton cascade* development proceeds then by propagating the partons along classical trajectories until they interact, i.e., collide (scattering or fusion process), decay (emission process) or coalesce to pre-hadronic composite states (cluster formation). Both space-like and time-like radiative corrections are included within the Leading-Log approximation. The relevant interaction probabilities are obtained from the well-known perturbative QCD cross-sections [23], and the coalescence probabilities of the Ellis-Geiger model [14–16], respectively. Both the production of partons and the emergence of pre-hadronic clusters through their coalescence are subject to an individually specific formation time $\Delta t_{p,c} = \gamma/M_{p,c}$ where $1/M_{p,c} = 1/\sqrt{k^2}$ is the proper decay time of off-shell partons or clusters with invariant mass M_p, respectively M_c, and $\gamma = E/M_{p,c}$ is the Lorentz factor.

(iii) The *afterburner hadron cascade* evolves similarly by propagating the pre-hadronic parton-clusters (those emerging from coalescence of materialized, interacted partons) along classical paths until they either scatter off or absorb other clusters or hadrons, or, until they convert into primary hadrons (cluster decay), followed by the hadronic decays into stable final state particles. The corresponding interaction probabilities are calculated from the 'additive quark model' [24] within which one can associate a specific cross-section for any pair of colliding hadrons according to their valence quark content. Cluster-cluster and cluster-hadron collisions are straightforward to

[†] We use the GRV structure function parametrization [22], which describes quite accurately the HERA data even at low Q^2 and very small x.

include in this approach, since in our model each pre-hadronic cluster that emerges from parton coalescence has a definite quark content, depending on the flavor of the mother partons. Hence, collisions among clusters and hadrons are treated on equal footing. Finally, the the decays of excited hadrons and resonances which are formed in these collisions, are sampled from the particle data tables [25]. Again, each newly produced hadron becomes a 'real' particle only after a characteristic formation time $\Delta t_h = \gamma/M_h$ depending on their invariant mass M_h and their energy through $\gamma = E/M_h$. Before that time has passed, a hadron must be considered as a still virtual object that cannot interact incoherently until it has formed according to the uncertainty principle.

(iv) The *beam remnants*, being the unscathed remainders of the initial nuclei, emerge from reassembling all those remnant primary partons that have been spectators without interactions throughout the evolution. The recollection of those yields two corresponding beam clusters with definite charge, baryon number, energy-momentum and positions as given by the sum of their constituents. These beam clusters decay into final-state hadrons which recede along the beam direction at large rapidities of the beam/target fragmentation regions. Again rescatterings, absorptive and emissive processes, as well as individual formation times, of the produced hadrons are accounted for as described in (iii).

We note that the spatial density and the momentum distribution of the particles are intimately connected: The momentum distribution continously changes through the interactions and determines how the quanta propagate in coordinate space. In turn, the probability for subsequent interactions depends on the resulting local particle density. Consequently, the development of the phase-space densities is a complex interplay, which - at a given point of time - contains implicitely the complete preceding history of the system.

B. CERN SPS: central $Pb + Pb$ collisions at $E_{cm} = 17$ A GeV

We first turn to the discussion of the results for $Pb + Pb$ collisions at beam momentum of $E_{beam} = 158$ GeV corresponding to $\sqrt{s}/A = 17$ GeV, as obtained from the computer simulations according to the above prescriptions.

1. Significance of parton production

To begin our discussion, we resurrect the first question that we raised in the Introduction, namely, how much of the nuclear collision energy is harnessed in truly partonic materialization with subsequent parton cascading, and how does the entwined evolution of partonic and hadronic matter components proceed.

Fig. 4 sheds light on the first part of the question, by exhibiting the relative importance of the truly partonic contribution to the final-state hadron yield. Shown is rapidity distribution for pion production $\pi^+ + \pi^- + \pi_0$ (representative for the bulk of produced hadrons) that results directly from parton materialization and the associated cascade evolution, as compared to the yield of final pions that arise from the soft fragmentation of the nuclear beam remnants which involves the spectator partons surviving from the initial state without materialization. The 'circles' give the total amount of produced pions, i.e. the sum of the contributions from the hadronization of materialized cascading partons via cluster formation and decay, plus the fragmentation of the nuclear beam remnants involving the remaining fraction of non-materialized spectator partons. The 'squares', on the other hand, represent the contribution that results solely from the latter beam fragmentation. The difference between the 'square' and 'circle' histograms therefore reflects the significance of the truly partonic dynamics of parton production and evolution. The essence of Fig. 4 is clear: even for $Pb + Pb$ collisions at CERN SPS $\sqrt{s}/A = 17$ GeV, the perturbative QCD parton production is in our model anything but negligible, contrary to wide-spread belief. In fact, it is responsible for about half of the final particle yield in the mid-rapidity region.

Fig. 5 elucidates the second part of the above questions, by detailing the time development of the particle production throughout the collision history. Shown are the time-dependent total numbers of materialized plus produced partons N_{parton}, of pre-hadronic clusters $N_{cluster}$ from parton-hadron conversion, and of produced hadrons N_{hadron}. The time $t = 0$ corresponds to the point of nuclear contact. Shortly thereafter parton materialization by hard scatterings produces a burst of partonic excitations N_{parton} up to $t \lesssim 0.1\ fm$. This initial production is then further enhanced by subsequent cascading and gluon emission, which reaches a maximum around $t \approx 1\ fm$. It follows then a decrease of the number of partons due to formation of pre-hadronic clusters via parton coalescence, thus feeding the buildup of $N_{cluster}$. The kink around $t \approx 3\ fm$ marks the setting in of soft cluster production from non-materialized initial-state partons which mimics the underlying fragmentation of the nuclear remnants. The following decays of these cluster into primary hadrons populate the yield N_{hadron}, continuing up to $t \approx 100\ fm$ due to the formation time of hadrons produced in the decays. As a consequence, a mixed system of clusters and already formed hadrons exists for a long time, during which the 'afterburner' cascading of interacting clusters and hadrons is active. The final hadron yield emerges only after about $t \approx 200\ fm$ when the free-streaming regime is reached.

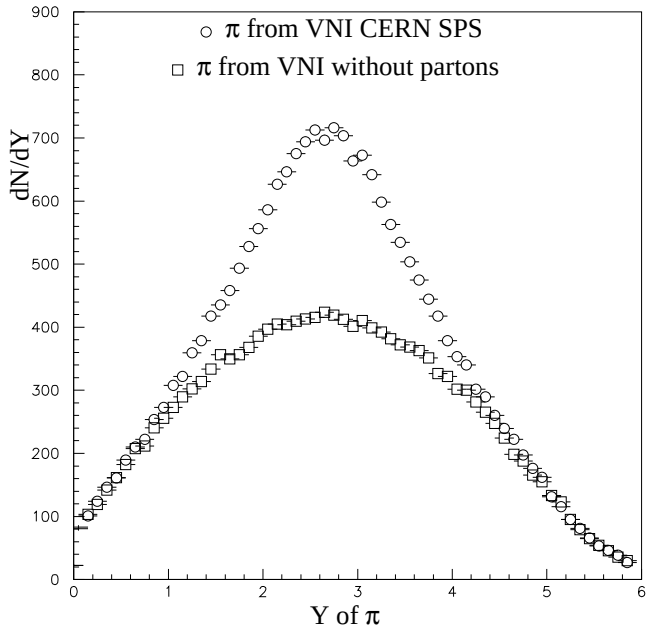

FIG. 4. Rapidity distribution of total pion yield in $Pb + Pb$ collisions at CERN SPS energy $E_{cm}/A = 17$ GeV: 'Circles' represent the sum of contributions from the parton cascade and the soft fragmentation of the beam remnants. 'Squares' indicate the contribution from the beam fragmentation only. The difference reflects the contribution of the parton cascade alone.

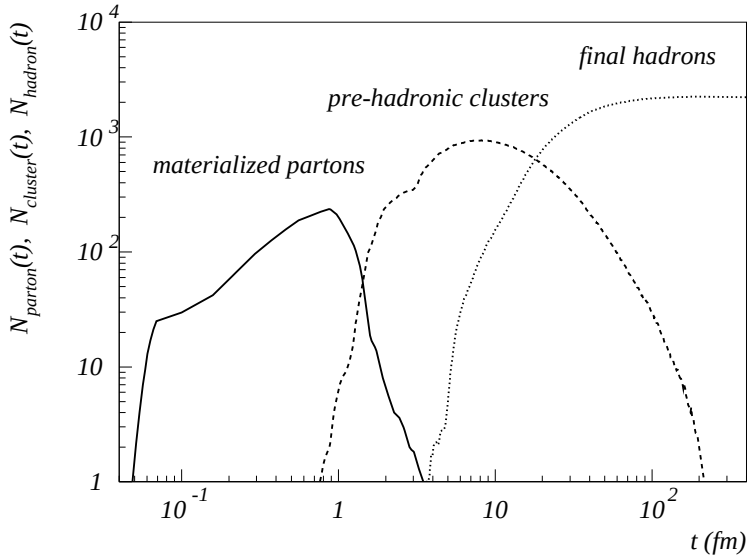

FIG. 5. Time evolution of the total numbers of produced partons N_p, pre-hadronic clusters N_c, and hadrons N_h during $Pb + Pb$ collisions at $E_{cm}/A = 17$ GeV. The time refers to the center-of-mass frame of the colliding nuclei.

2. Effects of hadronic 'afterburner' cascading

Next we turn to our second question of the Introduction, concerning the effects of the 'afterburner' cascade that involves re-interactions among produced pre-hadronic clusters and already formed hadrons. We discuss how these effects show up in the rapidity distributions and in the transverse mass spectra of final-state hadrons.

a) Rapidity spectra

Figs. 6 and 7 summarize the characteristic patterns of hadron production with and without 'afterburner' cascading of pre-hadronic clusters and hadrons after the parton cascade stage. Shown are the rapidity distributions of different meson and baryon species from $Pb + Pb$ collisions at CERN SPS energy. Throughout, we represent by 'circles' ('squares') the results from simulations without (with) 'afterburner' cascading. The solid-line histograms are results from VENUS, which we take as representative for the CERN SPS data (the corresponding real data were mostly not available for publication at this point).

Two remarkable features of the 'afterburner' cascading are inherent in the rapidity spectra, namely, the effect of pion and kaon absorption and associated resonance production, and, the effect of double, or even multiple, scattering of produced hadrons and their excitations. Firstly, the effect of π and K absorption in $\pi(K) + cluster$ or $\pi(K) + nucleon$ collisions is to transfer transverse energy from π or K via $\pi + C \rightarrow C^* \rightarrow X$ or $\pi + N \rightarrow N^* \rightarrow X$, $K + N \rightarrow S + X$, where N^* is a non-strange resonance such as Δ, and S a strange baryon, such as Λ, Σ, Ξ. These 'chemical' reactions in effect also decrease the primary π, K yield by feeding into the non-strange and strange baryon sector, respectively, as is evident from the spectra in Fig. 6 and 7. Secondly, the effect of rescatterings among clusters and hadrons generate additional deflection and slowing down of the particles, so that the final particle yields are concentrated more at central rapidities, as it would be the case without re-interactions. Both effects also give naturally rise to the phenomenon of 'baryon stopping', as discussed in the Introduction, since secondary interactions involving protons and neutrons from the nuclei shift those baryons towards mid-rapidity.

In Fig. 6, the pion distribution clearly exhibits the effect of absorption through 'afterburner' cascading by the reduction of the primary pion yield before(!) 'afterburner' cascading. The effect is evident throughout the entire rapidity range $0 \leq y \leq 6$, but is particularly prominent around mid-rapidity where it is about 30 %. In the kaon distribution, on the other hand, this absorption feature, although similarly present, is hardly visible, because it is counteracted by additional kaon production from meson-meson scatterings $M + M \rightarrow K + \overline{K}$ and meson-baryon collisions $M + B \rightarrow \overline{K} + S$ and $M + S \rightarrow K + B$. Consistent with the π and K absorption by nucleons is the loss of protons (both initial state and newly pair-produced ones) around $y \approx 1.5$ and $y \approx 3.5$. For the same reason, the amount of anti-protons from pair production is substantially decreased in the central region $2 \leq y \leq 4$.

In Fig.7, the patterns of Λ and $\overline{\Lambda}$ production is similar to the ones of p and $\overline{p}$. The simple reason is that the Λ's can be produced via kaon absorption by protons, or in pairs $\Lambda\overline{\Lambda}$ just as $p\overline{p}$. It is therefore no surprise that the Λ and $\overline{\Lambda}$ spectra are roughly proportional to the p and $\overline{p}$ densities, respectively. A very different behavior, however, is exibited in Σ and Ξ production, namely, a substantial increase through the 'afterburner' cascading of the primary yield emerging from the hadronization of the parton cascade. This strong population of Σ's and Ξ's arises naturally from the hadronic re-interactions and resonance production, as well as absorptive processes.

Overall we may conclude (viewing the solid-line histograms in Figs. 6 and 7 as reference to the shape of the actually measured distributions at CERN SPS) that the above effects show a general tendency of the 'afterburner' cascading to push the primary hadron spectra after the parton cascade towards the ones actually observed at CERN. The agreement of the results including the 'afterburner' cascade is quite decent.

b) Transverse mass spectra

The particle distributions in the transverse mass variable $m_\perp = \sqrt{m^2 + p_\perp^2}$ provide important information on the pattern and the degree of harnessing initial longitudinal momentum and energy into transverse direction. For example, in hadronic collisions, where re-interactions are negligible on both the parton and hadron level, a typical power-law behavior $\propto p_\perp^{-n}$ $(n = 4 - 6)$ at large $p_\perp$ is observed, which becomes increasingly prominent as the beam energy is increased. This characteristic $p_\perp$-production pattern indicates the contribution from perturbative QCD parton-parton collisions with associated (mini)jet production. On the other hand, in nucleus-nucleus collisions, the discussed effects of re-interactions among partons as well as hadrons, lead to a dampening of the large-$p_\perp$ tail as well as to an overall steepening, and hence to a characteristic exponential-type $p_\perp$-distribution. In our model, the effects of re-interactions on $p_\perp$-production may be exhibited by comparing nuclear collisions with and without 'afterburner' cascading.

Fig. 8 vividly reflects the intuitive expectation that rescatterings redistribute the particle momenta such that low-$p_\perp$ hadrons are accelerated in transverse direction by $p_\perp$ kicks towards larger $m_\perp$ and large-$p_\perp$ particles in the mean loose part of their transvere momentum through repeated collisions. This redistribution is nothing but the tendency of the multi-particle system to drive towards kinetic equilibrium through cascading. The 'equilibration effect', which twists the $m_\perp$-slopes, is visible in all three spectra, π, K, and p, most prominently however in the proton spectrum. The reason is that the initial-state protons carry large fractions of the longitudinal beam momentum, so that any scattering will cause a significant deflection with corresponding effect on the $m_\perp$-distibution. Pions and kaons on the other hand, are produced as secondaries mostly isotropic around mid-rapidity, and hence additional $p_\perp$ kicks wash away in the statistical mean, so that the effect on the $m_\perp$-spectra is small as compared to the case of protons.

Again, we may conclude from Fig. 8, that the inclusion of 'afterburner' cascading gives a fairly good agreement with the data (solid-lines), whereas the neglect of final-state interactions in the case of protons is clearly off the data.

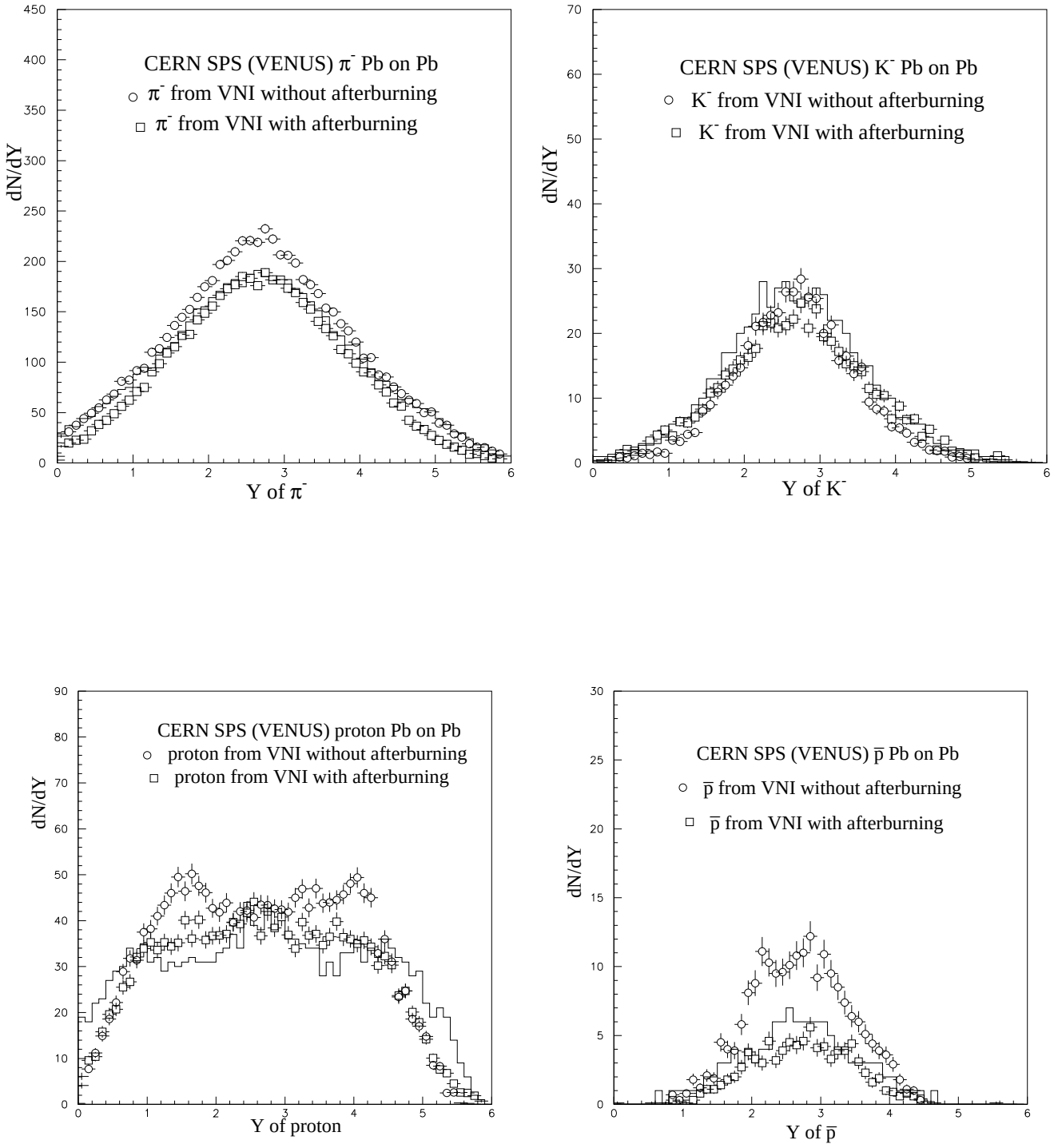

FIG. 6. Rapidity spectra for π^-, K^-, p and $\bar{p}$ without (circles) and with (squares) 'afterburner' cascading in $Pb + Pb$ collisions at CERN SPS energy.

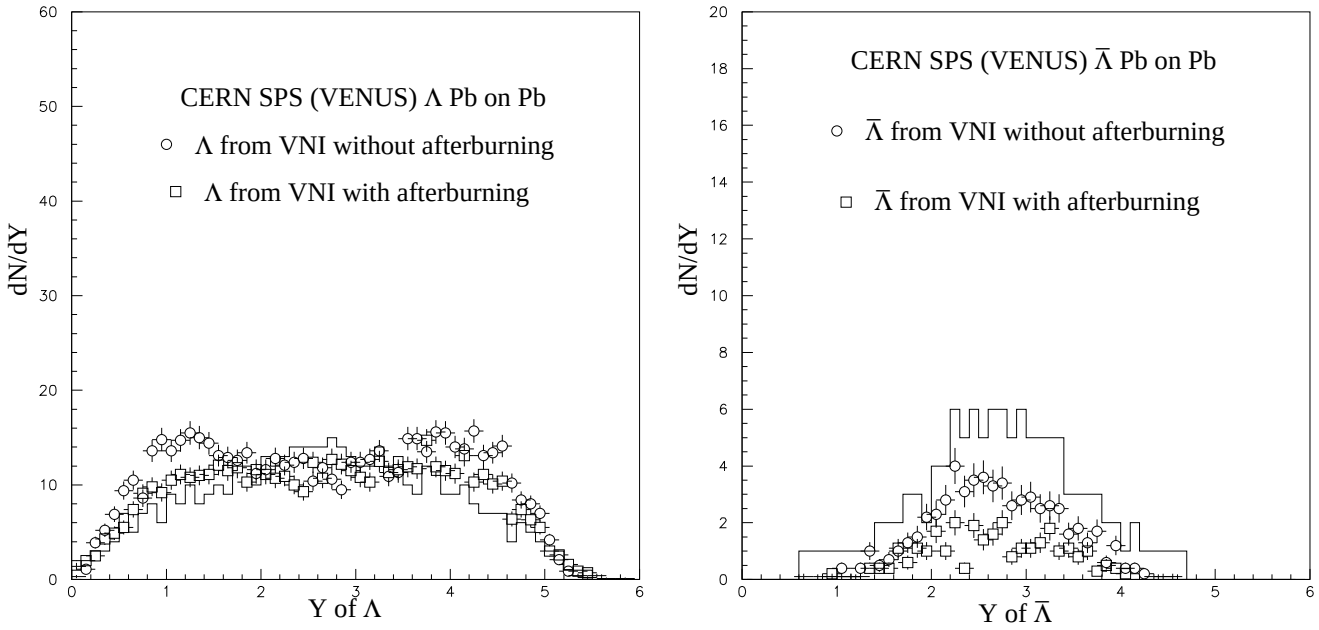

a

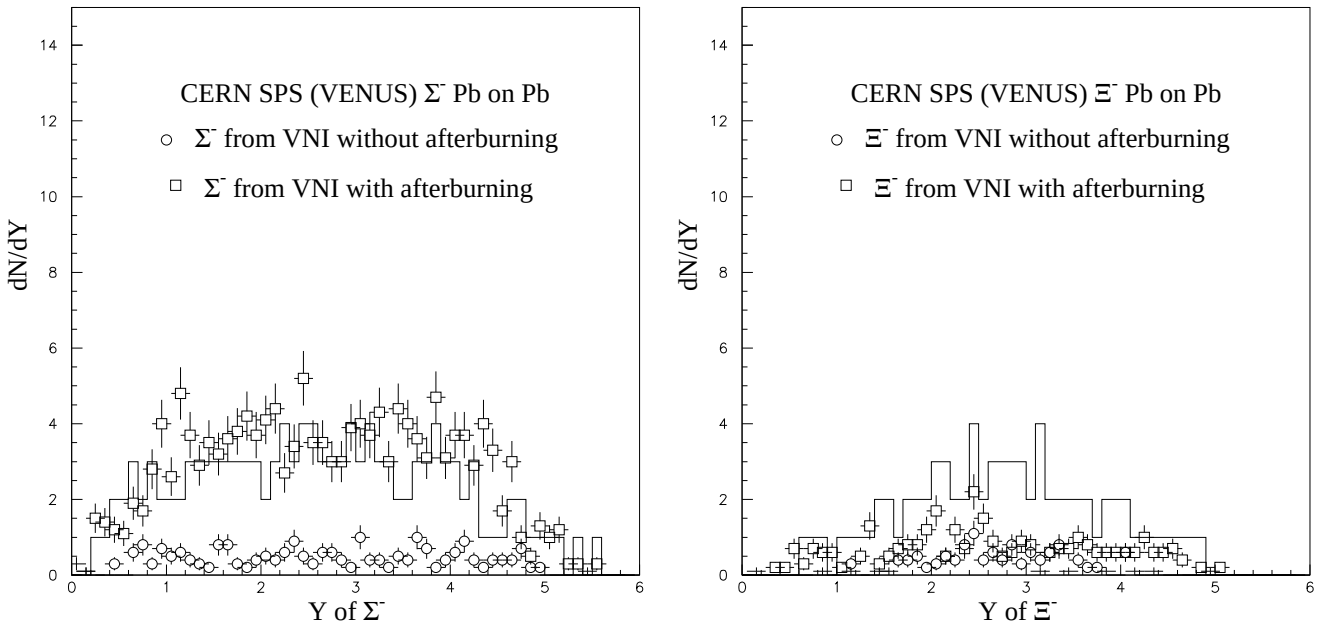

FIG. 7. Rapidity spectra for Λ, $\bar{\Lambda}$, Σ^{-}, Ξ^{-} without and with afterburner' cascading in $Pb + Pb$ collisions at CERN SPS energy.

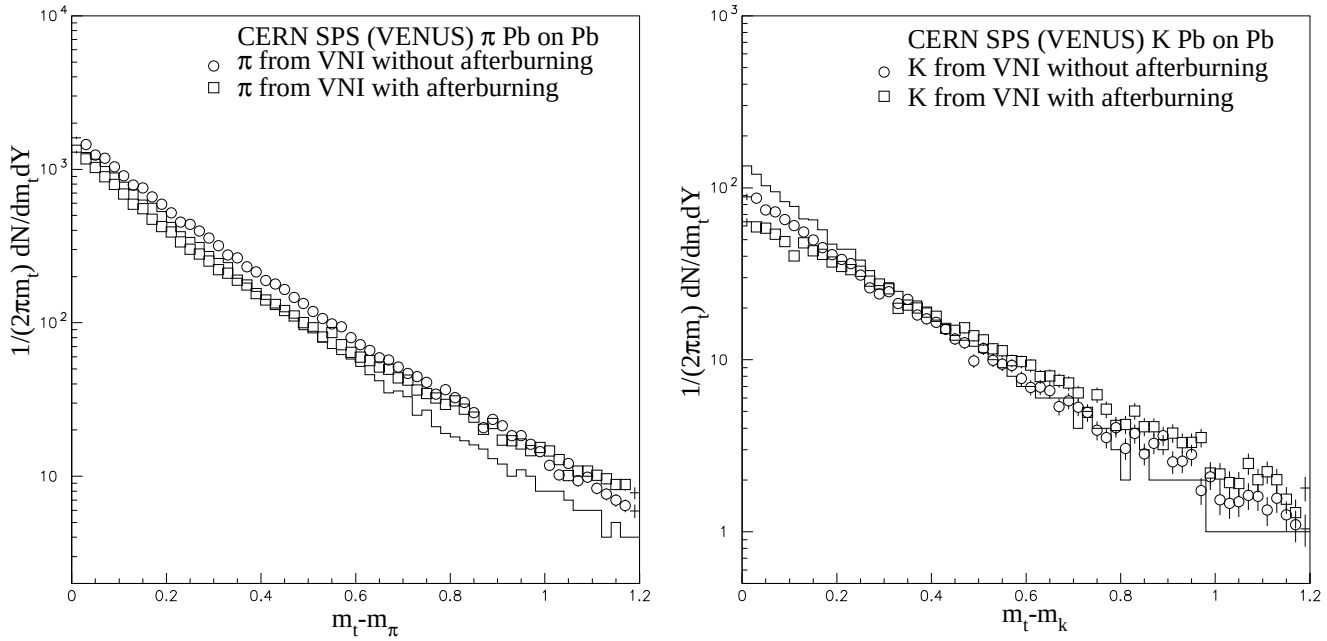

a

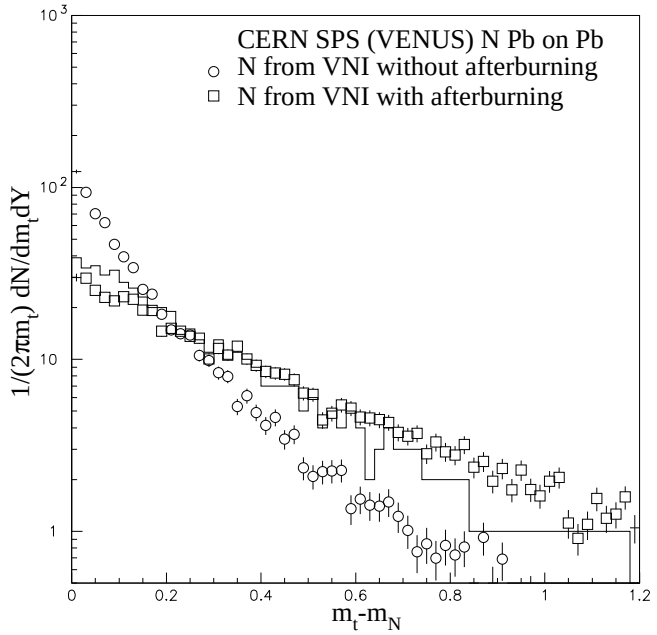

FIG. 8. Transverse mass spectra for $\pi \equiv \pi^+ + p^- + \pi^0$, $K \equiv K^+ + K^-$, and $N \equiv p + n$, without and with afterburner' cascading in $Pb + Pb$ collisions at CERN SPS energy.

C. RHIC: central $Au + Au$ collisions at $E_{cm} = 200$ A GeV

After having gained insight within our model on the overall particle production features at the CERN SPS, we now address $Au + Au$ collisions at more than an order of magnitude larger collision energy $\sqrt{s}/A = 200$ GeV.

1. Significance of parton production

As in our previous discussion in Sec. IIIB, Fig. 9 illustrates the rapidity distributon of total pion production ('circles'), resulting from the truly perturbative QCD component of parton materializaton and associated cascading, and from the underlying non-perturbative component due to soft fragmentation of the nuclear beam remnants that consist of the non-materialized initial state partons ('squares'). Confronting this plot for RHIC energy with the analogous Fig. 5 for CERN SPS energy, one observes that the perturbative parton component becomes the dominant source for particle production at central rapidities, yielding about 70-80 % of the final hadrons in $|y| \leq 1$.

Another important feature is the shape of the y-distribution at RHIC, which is considerably stronger peaked than at CERN SPS, due to the increased production of low-energy gluons in the former case, both by the stronger gluon presence in the inital nuclei at the smaller Bjorken-x values probed, as well as by more copious gluon emision during the parton cascading due to larger momentum transfers of parton collisions.

Moreover, in effect, there is no plateau-like structure visible at mid-rapidity, even if $|y| \leq 1$. This is in strict contrast to the wide-spread hypothesis that an approximate boost-invariant Bjorken picture [26] with uniform rapidity plateau at central reapidities should emerge. Because of the peak structure of the rapidity distribution the density $dN/dy|_{y=0}$ is substantially larger than commonly assumed, implying a very high particle density at $y \approx 0$. However, it drops off rapidly, so that the total, y-integrated yield is much less dramatic.

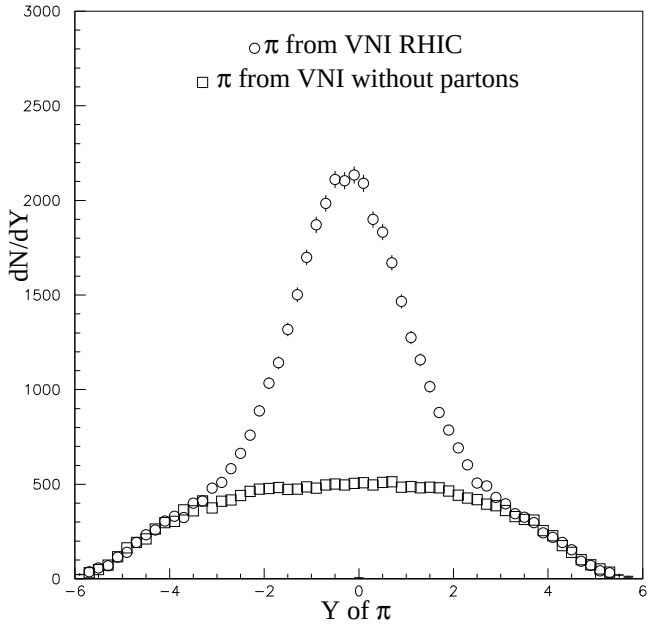

FIG. 9. Rapidity distribution of total pion yield in $Pb + Pb$ collisions at CERN SPS energy $E_{cm}/A = 17$ GeV: 'Circles' represent the sum of contributions from the parton cascade and the soft fragmentation of the beam remnants. 'Squares' indicate The contribution from the beam fragmentation only. The difference reflects the contribution of the parton cascade alone.

2. Effects of hadronic 'afterburner' cascading

Figs. 10 and 11 exhibit the effects of the 'afterburner cascading' at RHIC, including as before the re-interactions among prehadronic clusters and hadrons, in correspondence to Figs. 6 and 7 for CERN SPS.

Fig. 10, which shows the rapidity distributions of final-state pions, kaons and protons, indicates that the 'afterburner' cascading is equally important at RHIC as it is at CERN SPS, neither is it less, nor seems there to be significant increase of hadronic cascading at RHIC as one might have expected due to a factor of 10 larger energy per nucleon available. However, in view of the previous Fig. 9, this is understandable, because a larger amount of the initial total collision energy is harnessed during the parton cascade stage. If that holds true at even larger energies, this would imply a certain universal, energy-independent character of the 'afterburner' cascading.

The general patterns of the 'afterburner' cascading effects at RHIC in Fig. 10 and 11 resembles the ones of Fig. 6 and 7 for CERN SPS, however, there is an important difference, namely the fact that at RHIC the nucleons, mostly originating from the nuclear beams, are pre-dominantly appearing in the rapidity intervals $-4 \leq y \leq -2$ and $2 \leq y \leq 4$, as is evident from the plot of the proton distribution in Fig. 11. Hence, the separation between the baryon-rich regions in the forward and backward hemispheres is twice as large as at the CERN SPS (c.f. Fig. 6), where they peak within $1 \leq y \leq 2$ and $4 \leq y \leq 5$, corresponding to center-of-mass rapidities $-2 \leq y \leq -1$ and $1 \leq y \leq 2$. As a consequence of the large density of primary nucleons at RHIC in the rapidity intervals $-4 \leq y \leq -2$ and $2 \leq y \leq 4$, an enhanced production of pions and kaons is generated by re-interactions of primary nucleons: The π and K spectra in Fig. 10 with 'afterburner' cascading ('squares') exhibit shoulders in these baryon-rich rapidity intervals, as compared to the case without ('circles'). The opposite is true for the proton distibution in Fig. 11, which becomes substantially diminished in these y-regions after inclusion of the 'afterburner' cascading, because secondary collisions involving nucleons, such as $N + \pi \rightarrow N* + \pi \rightarrow n\,\pi + X$ eat away protons and neutrons, feeding the pion yield, for instance.

Also shown in Fig. 11 are the y-spectra of $\bar{p}$, Λ, and Σ for RHIC. As compared to Fig. 7, which shows the corresponding spectra for CERN SPS, one recognizes again that the main activity for Λ and Σ production is concentrated in $-4 \leq y \leq -2$ and $2 \leq y \leq 4$, because the nucleon density is the highest there so that nucleon-induced production of these particles is enhanced. In contrast to this, the production of $\bar{p}$ (and similarly for $\bar{\Lambda}$, not shown here), is concentrated in the central region $|y| \leq 2$, as one would expect, because the $\bar{p}$ (or $\bar{\Lambda}$) are produced via pair-production, rather than by pion or kaon absorption of high-momentum nucleons.

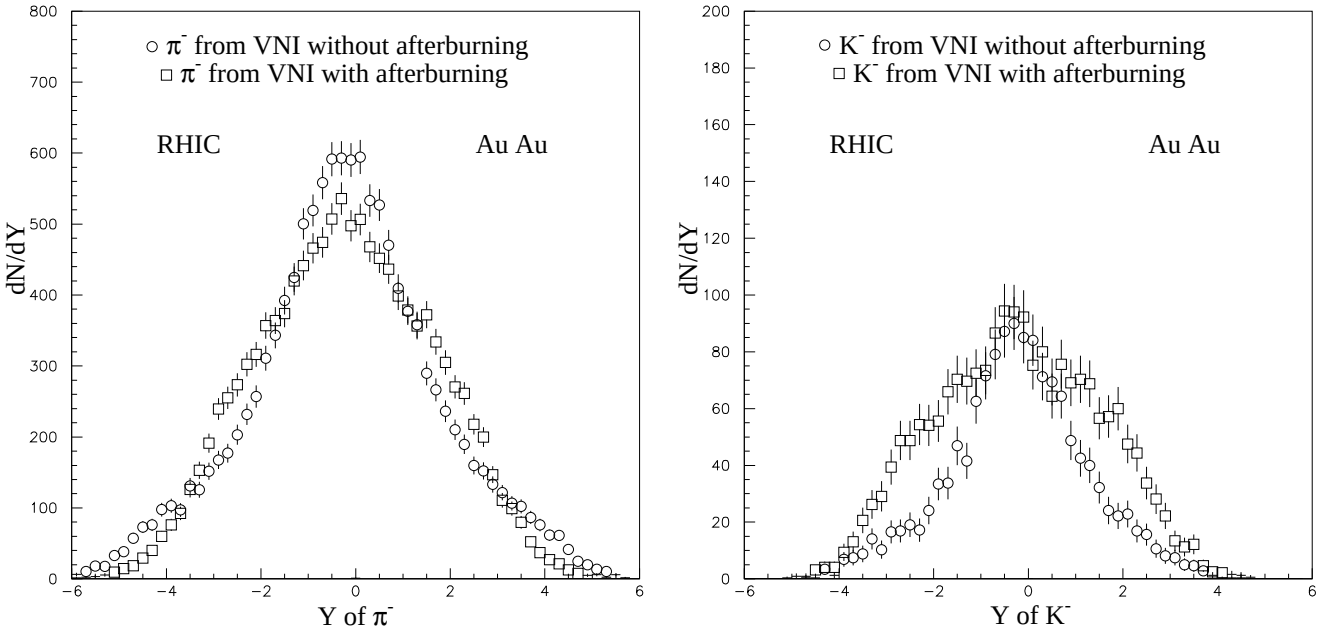

FIG. 10. Rapidity distributions π^- and K^- without (circles) and with (squares) afterburner' cascading in $Au+Au$ collisions at RHIC energy.

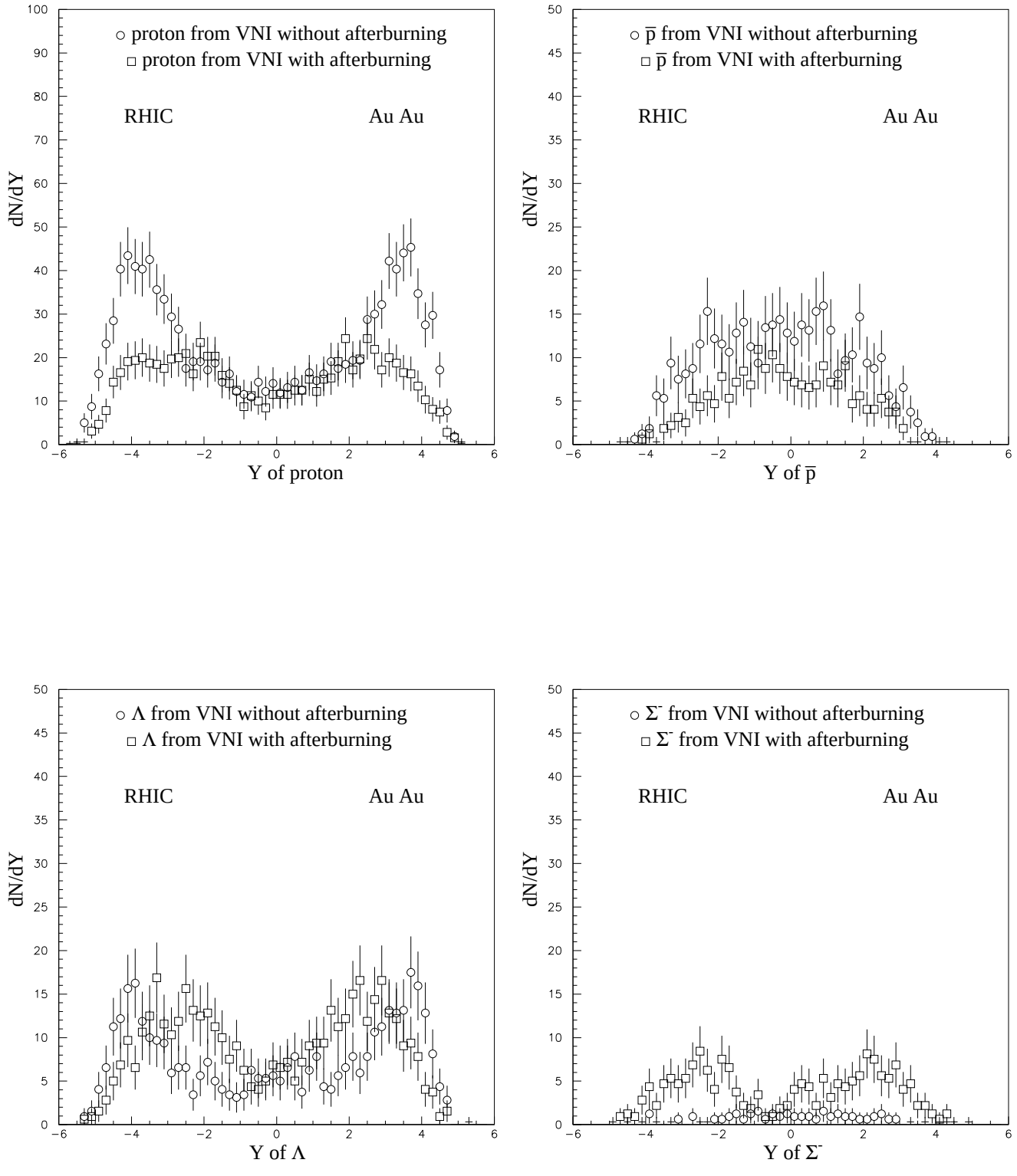

FIG. 11. Rapidity distributions of p, $\bar{p}$, Λ and Σ^{-}, without and with afterburner' cascading in $Au + Au$ collisions at RHIC energy.

IV. SUMMARY

In this work we have analysed $Pb + Pb$ collisions at the CERN SPS with beam energy per nucleon 158 GeV ($\sqrt{s}/A = 17$ GeV) and $Au + Au$ collisions at RHIC with collider energy $\sqrt{s}/A = 200$ GeV, by performing Monte Carlo simulations within the framework of a space-time model that involves the dynamical interplay between parton production, evolution, parton-cluster formation, and 'afterburner' cascading of formed pre-hadronic clusters plus hadron excitations. We see this study as a first exemplary attempt to describe high-energy nuclear collisions on the microscopical level of the space-time history of parton and hadron degrees of freedom based on QCD and supplemented by phenomenology. We developed a 'joint venture' of the Monte Carlo programs VNI and HIJET that allowed us to trace in detail the time evolution of nuclear collisions in both position and momentum space, from the instant of nuclear overlap to the final yield of particles.

Our main conclusions may be summarized as follows:

(i) The perturbative QCD parton production and parton cascading provides an important contribution to particle production at central rapidities. In effect this partonic component almost doubles the amount of pions around $y = 0$, as compared to sole contribution from the underlying soft fragmentation of the nuclear beam particles.

(ii) The 'afterburner' cascading of pre-hadronic clusters and already formed hadrons which emerge from the parton cascade, as well as from the soft fragmentation of the nuclear beam remnants, turns out to be most important in the central phase-space region around mid-rapidity where the particle densities are the largest. The two main mechanisms of the 'afterburner' cascading are pion/kaon absorption by, and multiple scattering of clusters and hadrons.

(iii) The overall agreement of our model calculations including the 'afterburner' cascading with the observed particle spectra at the CERN SPS is fairly good, whereas the neglect of the final-state interactions among hadronic excitations deviates significantly from the data.

(iv) In heavy-ion collisions at RHIC, we have absolutely no indication of a plateau-form at mid-rapidity, not even in a narrow interval at $y = 0$. Instead the bulk of particles strongly peaks leading to a very high particle density $dN/dy|_{y=0}$, but rapidly dropping off for y values different from zero.

(v) In RHIC collisions, we find that an essentially baryon-free region between $-2 \leq y \leq 2$ is created, whereas the the high-momentum nucleons appear mainly in the rapidity intervals $-4 \leq y \leq -2$ and $2 \leq y \leq 4$ and produce two baryon-rich peaks in the forward and backward hemispheres, respectively.

Especially the latter two points would have important consequencees: If both these effects indeed turn out so drastic at RHIC as compared to CERN SPS, then this would imply very favorable conditions for the formation of a baryon-free quark-gluon plasma in the central rapidity region, and possibly even a baryon-rich plasma in the nucleon-dense fragmentation regions.

In view of the semi-classical particle picture underlying our approach, we may say that the bulk features of particle production at CERN SPS can actually be described without introducing additional prescriptions to accomodate the observed physics (we emphasize that we have not attempted to fine-tune our model to fit the data). On the other hand, an investigation of more sensitive observables may well fail, in which case we could identify this as truly new physics beyond a simple particle-cascade description. In any case it would be desirable to extend and deepen this study by looking for instance at nuclear collisions with other beams and different energy, or at proton-nucleus collisions. We intend to pursue this project in the near future.

Notwithstanding, at this point we may take the decent description of the CERN $Pb+Pb$ data by our mixed parton-hadron cascade as encouragement to look forward to RHIC or even LHC. Since the relative importance of partonic and hadronic degrees are regulated by the multi-particle dynamics itself, our model should provide a smooth extrapolation to these future nuclear collisions beyond the CERN SPS.

ACKNOWLEDGEMENTS

This work was supported in part by the D.O.E under contract no. DE-AC02-76H00016.

REFERENCES

[1] G. Wolf, in the proceedings of the *International Workshop on Deep Inelastic Scattering*, Eilat, Israel, 1994.
[2] X.-N. Wang and Z. Huang, preprint LBL-39742, hep-ph/9701227.
[3] D. Kharzeev, Nucl. Phys. **A610**, 418c (1996).
[4] B. Müller, Rep. Prog. Phys. **58**, 611 (1995);
J. W. Harris and B. Müller, Ann. Rev. Nucl. Part. Sci. **46**, 71 (1997).
[5] B. Andersson, G. Gustafson and B. Nilsson-Almquist, Nucl. Phys. **B281**, 289 (1987);
B. Nilsson-Almquist and E. Stenlund, Computer Phys. Comm. **43** (1987), 387;
B. Lörstad, Int. J. Mod. Phys. **A12**, 2861 (1989).
[6] K. Werner, Z. Phys. **C42**, 85 (1989); Phys. Rep. **232**, 87 (1993).
[7] H. Sorge, H. Stöcker, and W. Greiner, Nucl. Phys. **A498**, 567c (1989); Ann. Phys. **192**, 266 (1989).
[8] A. Capella, U. Sukhatme, C.-I. Tan, and J. Tran Tranh Van, Phys. Rep. **236**, 225 (1994)
[9] X. N. Wang and M. Gyulassy, Phys. Rev. **D44**, 3501 (1991); Comp. Phys. Com. **83**, 307 (1994).
[10] K. Geiger, preprint BNL-63632, hep-ph/9701226 (to appear in Comp. Phys. Com.).
[11] K. Geiger, Phys. Rep. **258**, 238 (1995).
[12] A. Shor and R. Longacre, Phys. Lett. **B218**, 100 (1989);
R. Longacre, in the proccedings of *Heavy ion physics at the AGS*, eds. G. S. F. Stephans, S. G. Steadman, and W. Kehoe, MIT report MITLNS-2158, 1993. Phys. Lett. **B218**, 100 (1989).
[13] K. Geiger, Phys. Rev. **D54**, 949 (1996);
[14] J. Ellis and K. Geiger, Phys. Rev. **D54**, 949 (1996),
[15] J. Ellis and K. Geiger, Phys. Rev. **D54**, 1755 (1996).
[16] J. Ellis, K. Geiger, and H. Kowalski, Phys. Rev. **D54**, 5443 (1996).
[17] L. V. Gribov, E. M. Levin, and M. G. Ryskin, Phys. Rep. **100**, 1 (1983);
E. M. Levin, and M. G. Ryskin, Phys. Rep. **189**, 267 (1990).
[18] K. Geiger, preprint BNL-63232, hep-ph/9611400.
[19] Yu. L. Dokshitzer, D. I. Dyakonov, and S. I. Troyan, Phys. Rep. **58**, 269 (1980).
[20] K. Konishi, A. Ukawa, and G. Veneziano, Nucl. Phys. **B157**, 45 (1979).
[21] A. Bassetto, M. Ciafaloni and G. Marchesini, Phys. Rep. **100**, 203 (1983).
[22] M. Glück, E. Reya and A. Vogt, Z. Phys. **C48**, 471 (1990); Z. Phys. **C67**, 433 (1995).
[23] See e.g.: R. D. Field, *Applications of Perturbative QCD*, Frontiers in Physics **77**, (Addison-Wesley, 1989).
[24] See e.g.: F. Wagner, in the proccedings of *11th Rencontre de Moriond*, Flaine, France, published in Moriond Conf.1976:217 (QCD161:R34:1976:V.1)
[25] See e.g.: Particle Data Group, *Review of Particle Properties*, Phys. Rev. **D50**, 1173 (1994).
[26] J. D. Bjorken, Phys. Rev. **D27**, 140 (1983).

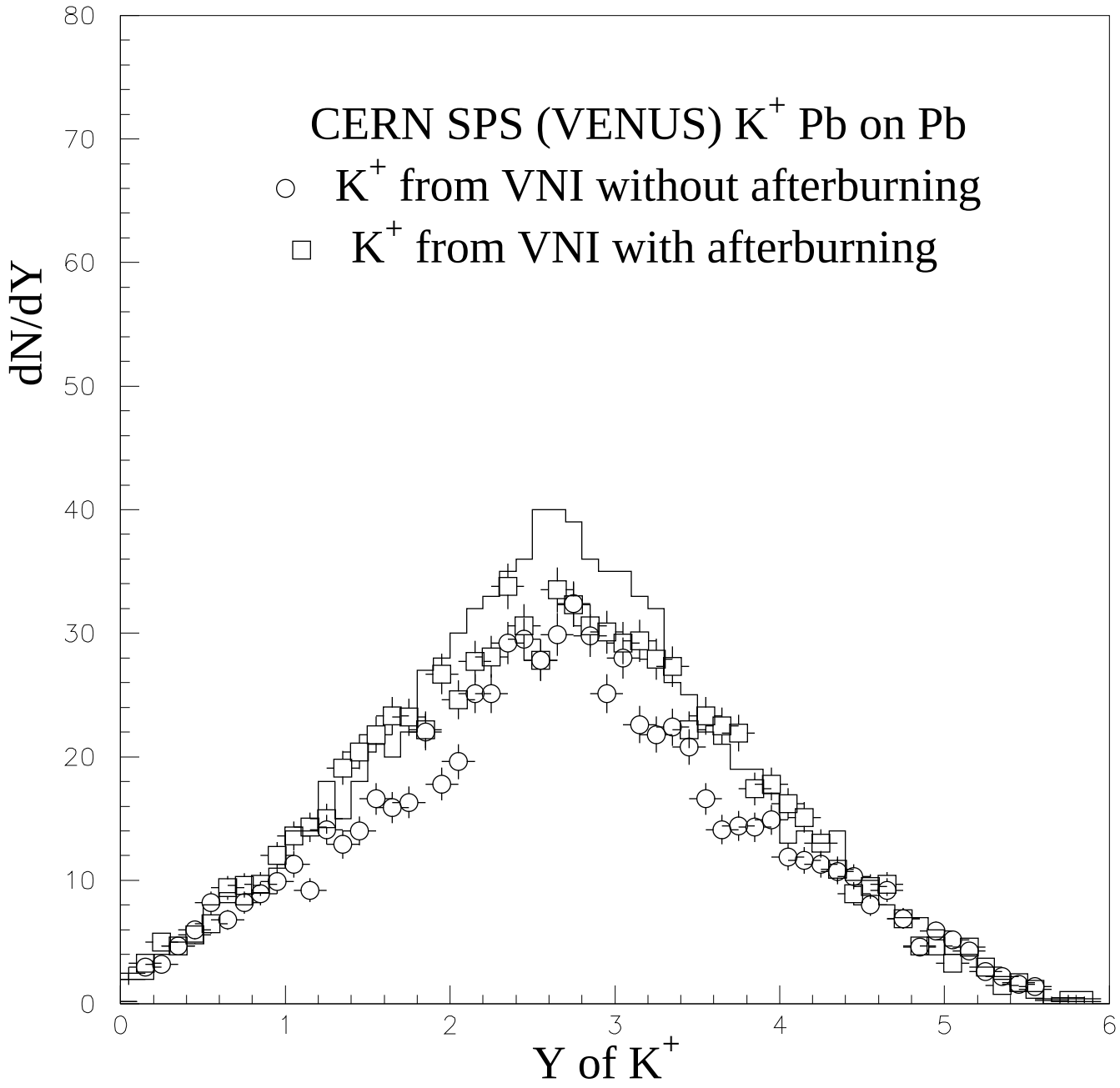
CERN SPS (VENUS) K+ Pb on Pb
K+ from VNI without afterburning
K+ from VNI with afterburning
dN/dY
Y of K+
0
10
20
30
40
50
60
70
80
0
1
2
3
4
5
6

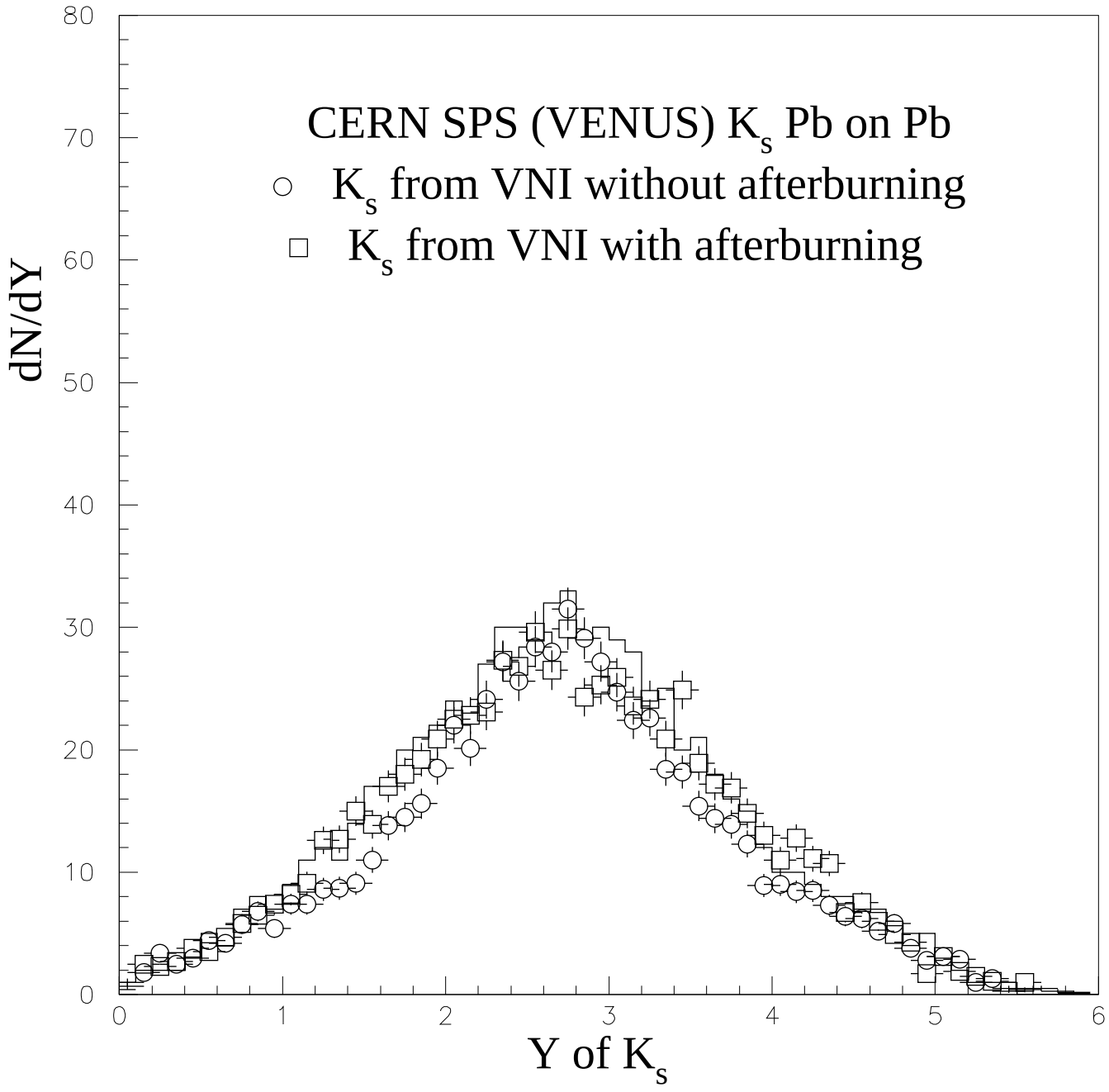
CERN SPS (VENUS) K_s Pb on Pb
○ K_s from VNI without afterburning
□ K_s from VNI with afterburning
dN/dY
Y of K_s
0
10
20
30
40
50
60
70
80
0
1
2
3
4
5
6

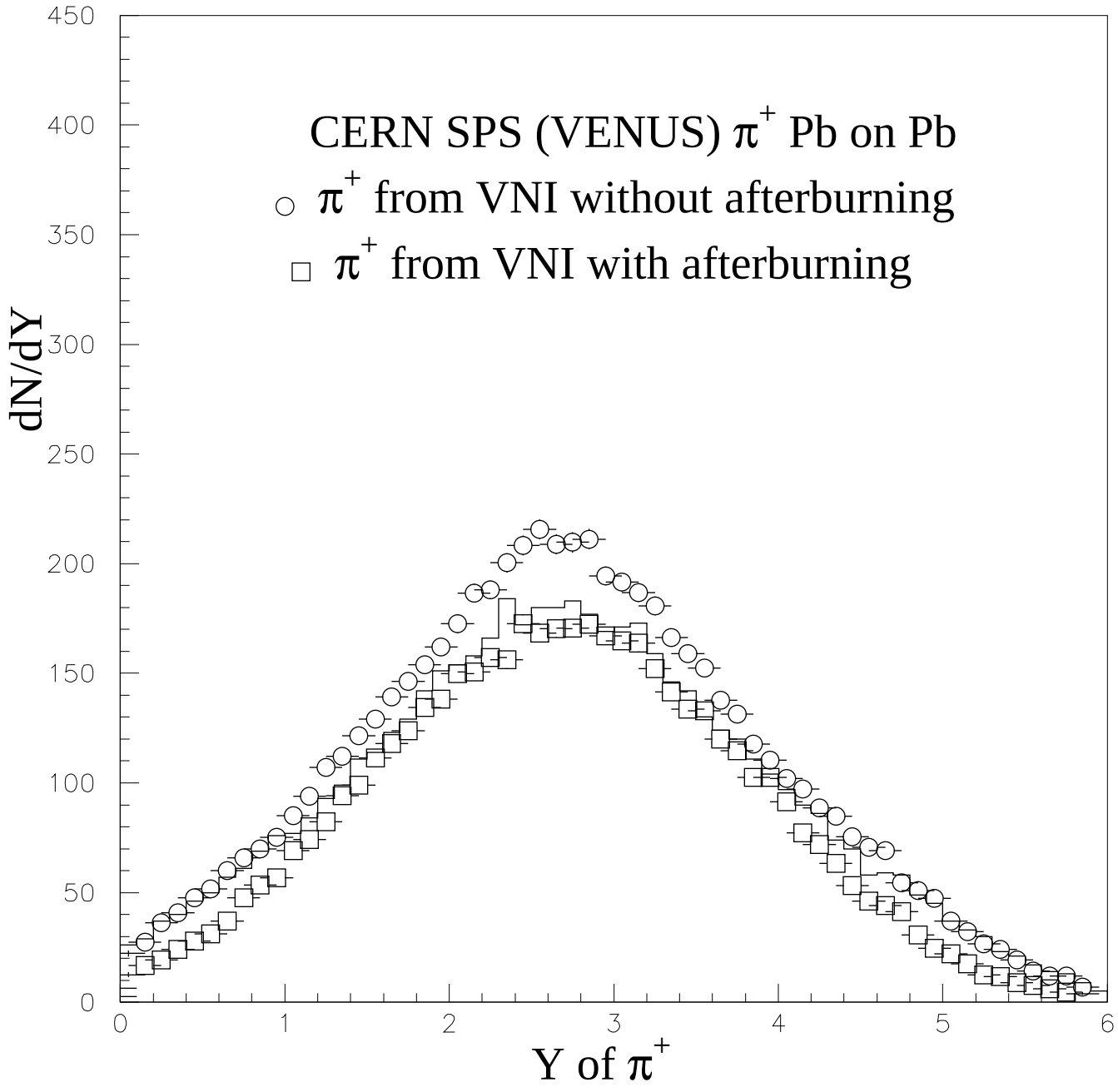
CERN SPS (VENUS) π^+ Pb on Pb
○ π^+ from VNI without afterburning
□ π^+ from VNI with afterburning
dN/dY
Y of π^+
0
50
100
150
200
250
300
350
400
450
0
1
2
3
4
5
6

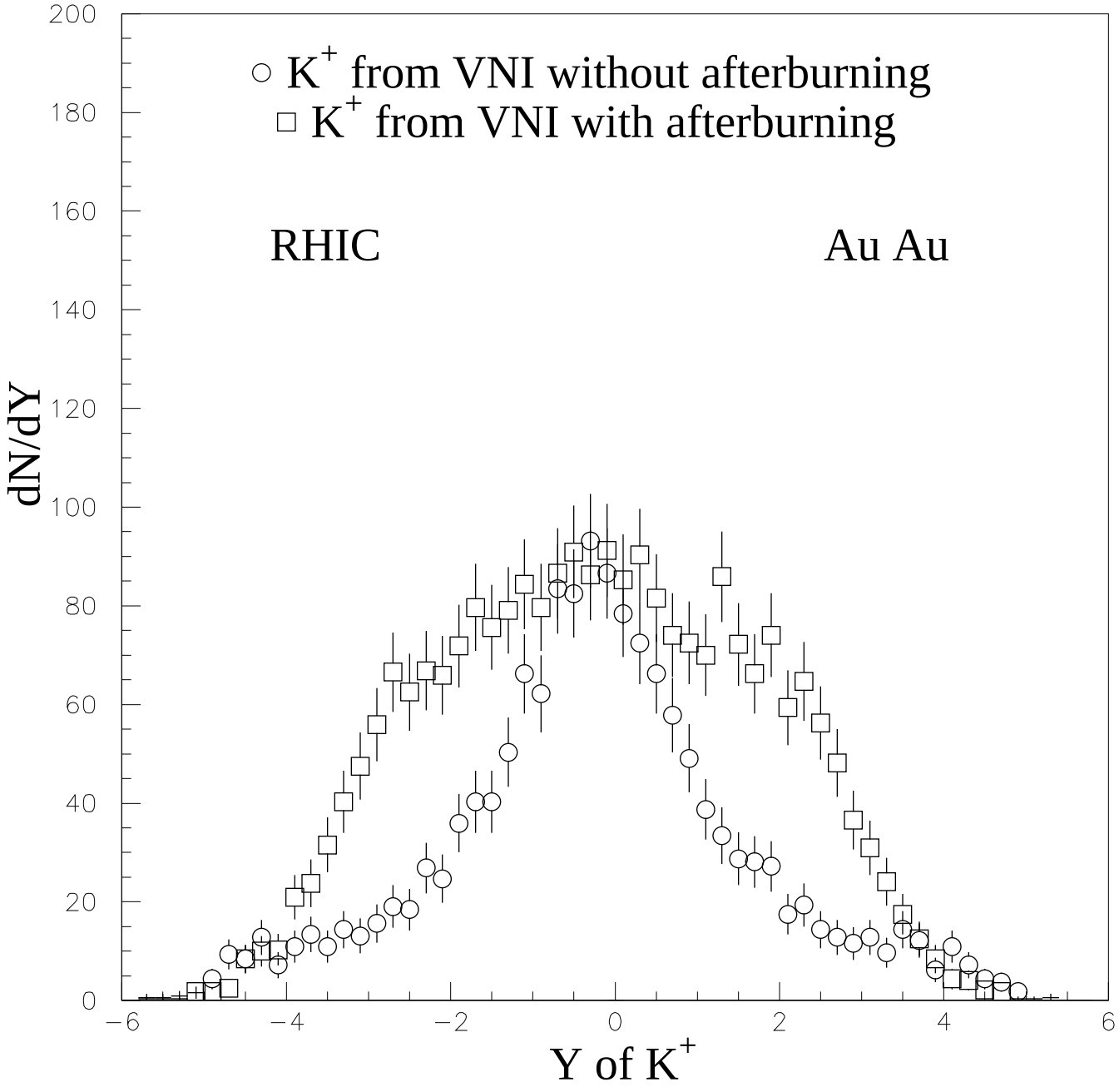
○ K+ from VNI without afterburning
□ K+ from VNI with afterburning
RHIC
Au Au
dN/dY
Y of K+
200
180
160
140
120
100
80
60
40
20
0
−6
−4
−2
0
2
4
6

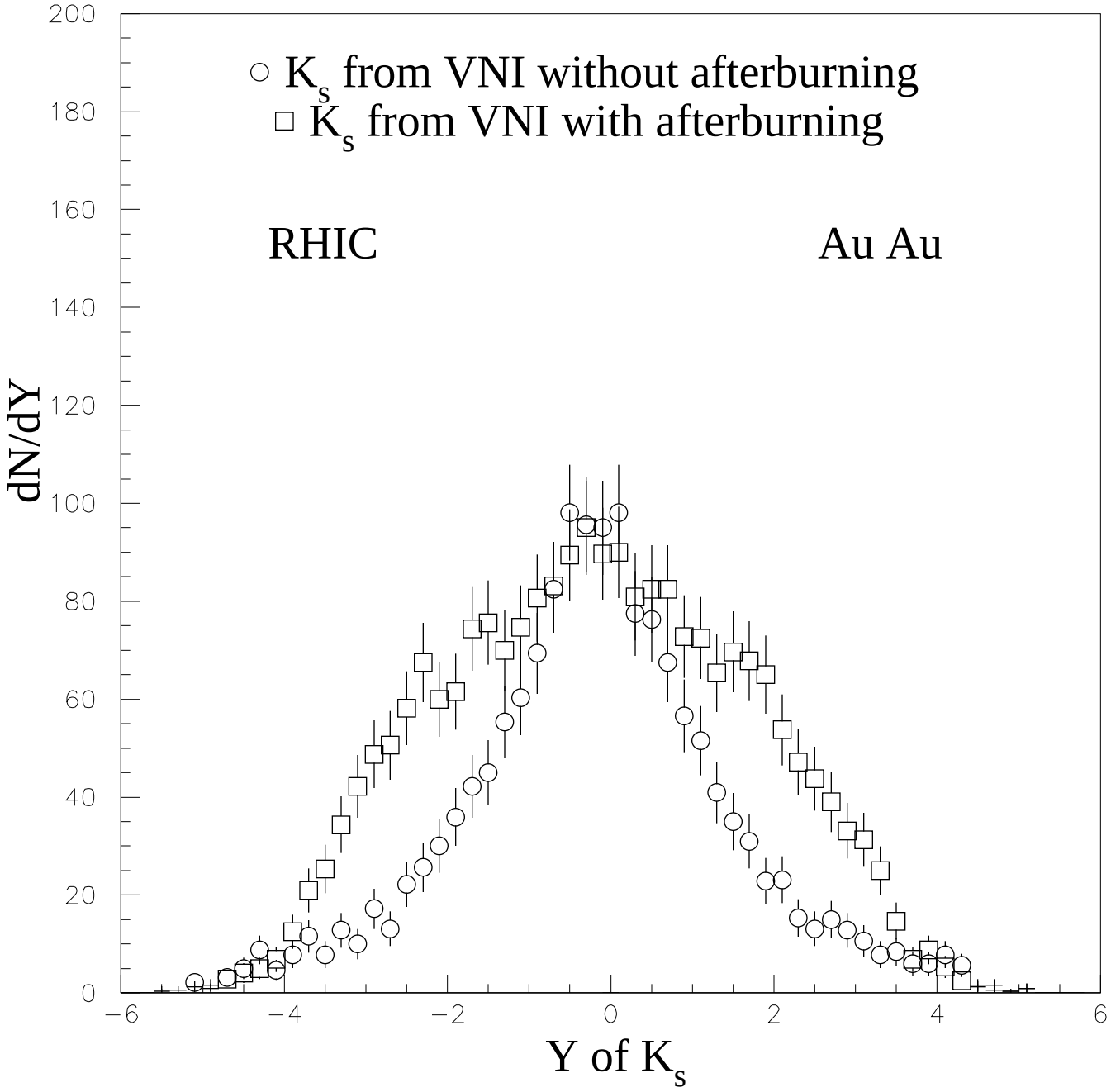
○ K_s from VNI without afterburning
□ K_s from VNI with afterburning
RHIC
Au Au
dN/dY
Y of K_s
200
180
160
140
120
100
80
60
40
20
0
−6
−4
−2
0
2
4
6

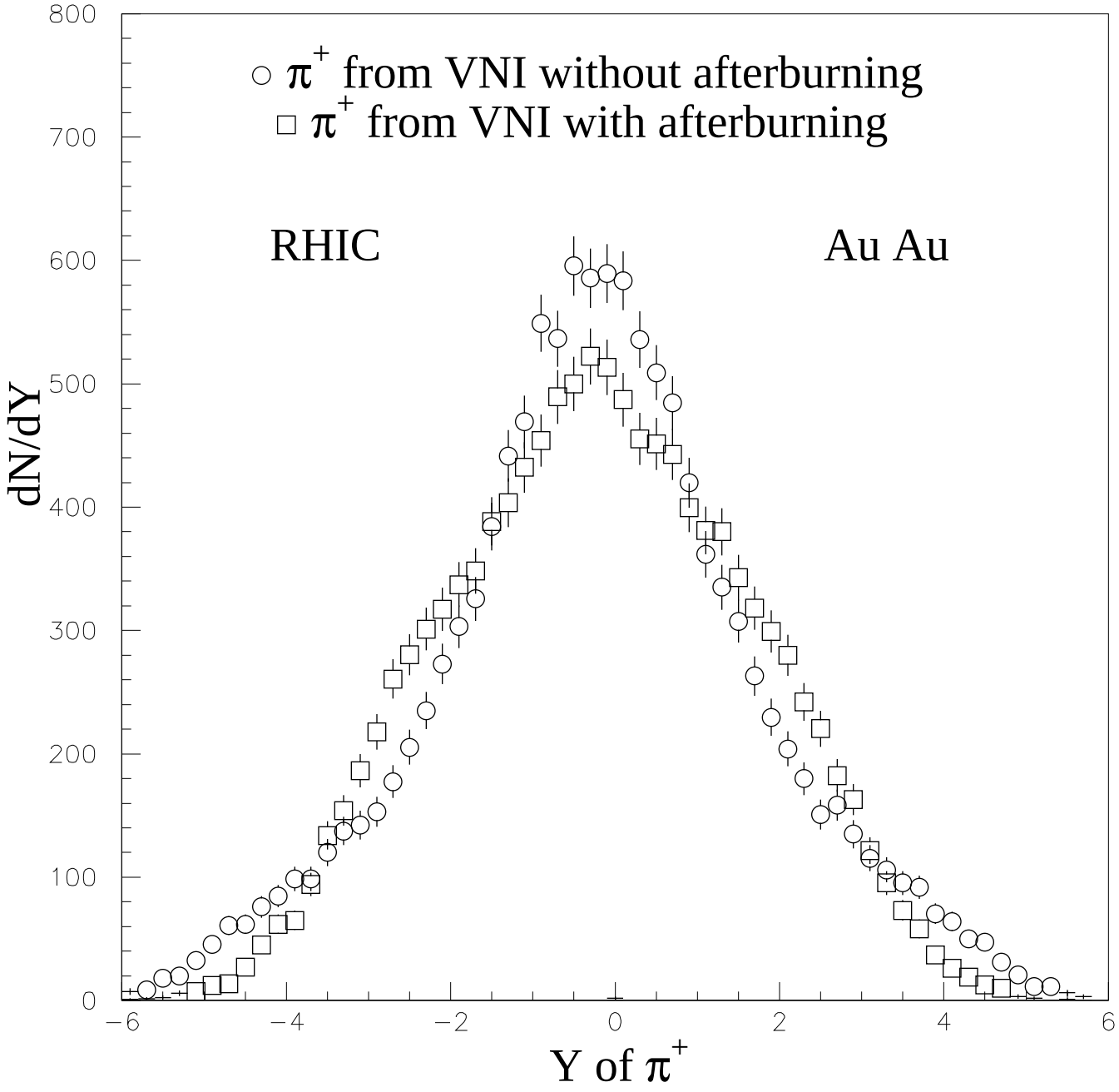
○ π+ from VNI without afterburning
□ π+ from VNI with afterburning
RHIC
Au Au
dN/dY
Y of π+
800
700
600
500
400
300
200
100
0
−6
−4
−2
0
2
4
6

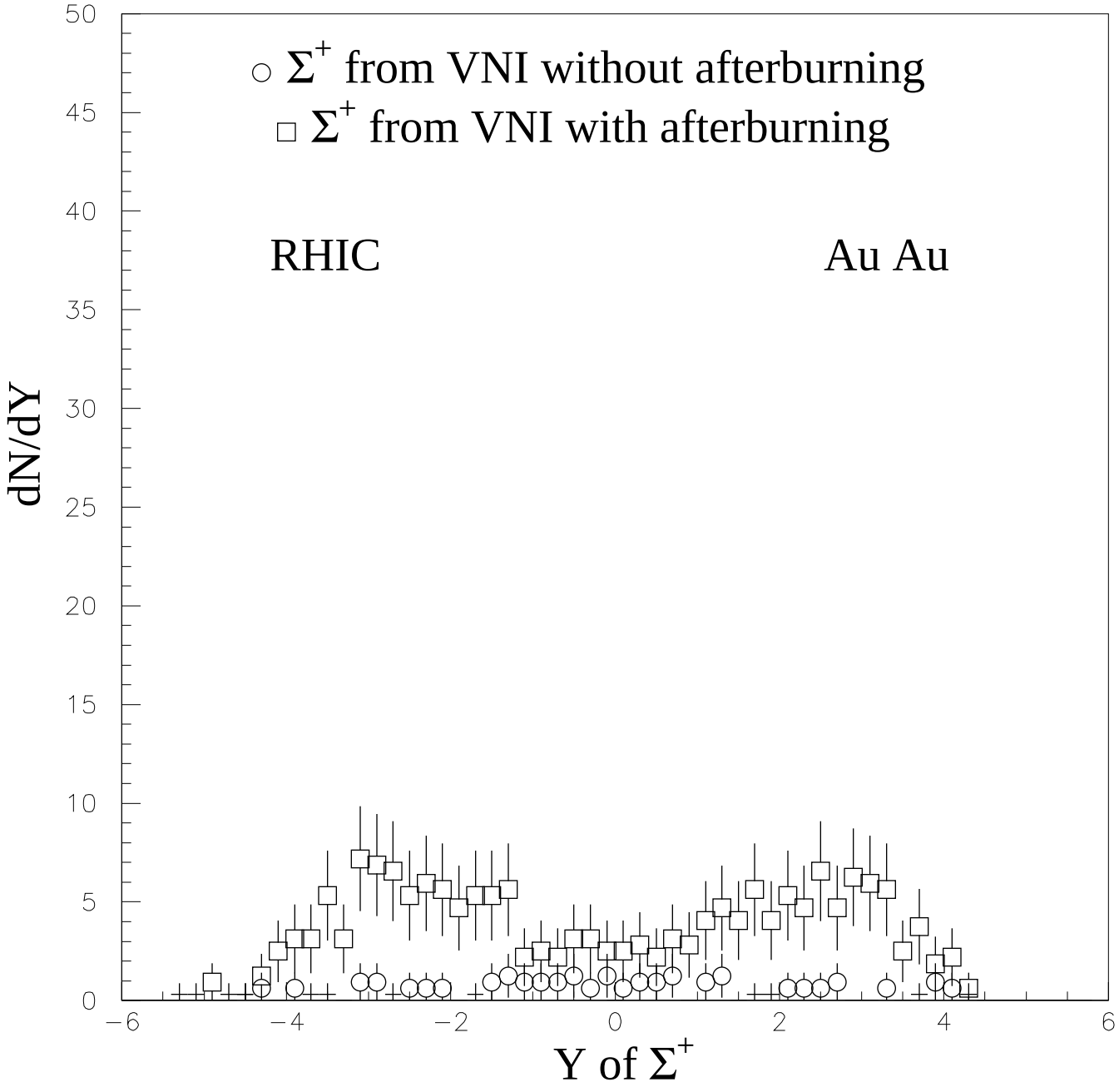
○ Σ+ from VNI without afterburning
□ Σ+ from VNI with afterburning
RHIC
Au Au
dN/dY
Y of Σ+
0
5
10
15
20
25
30
35
40
45
50
−6
−4
−2
0
2
4
6

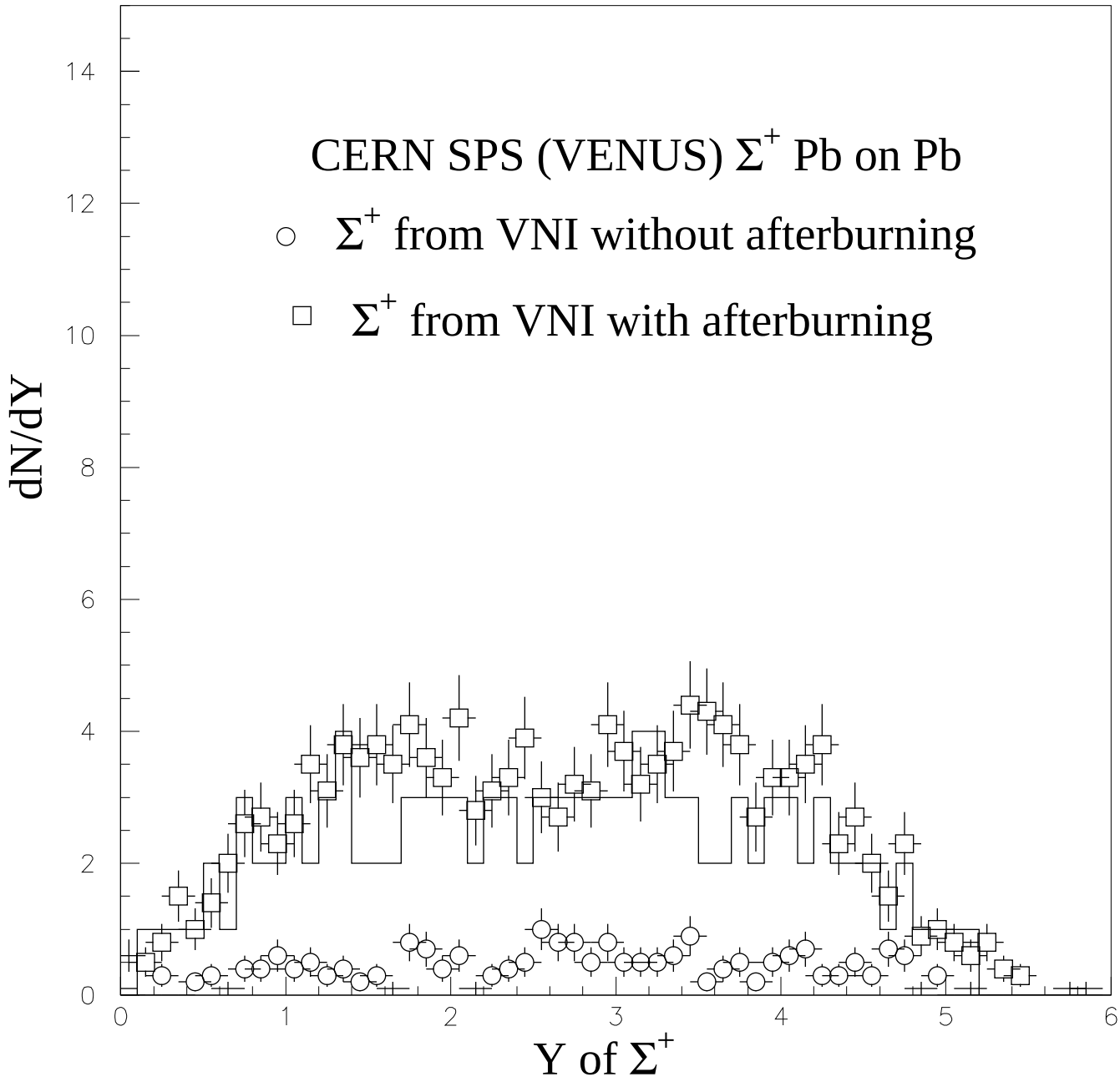
CERN SPS (VENUS) Σ+ Pb on Pb
○ Σ+ from VNI without afterburning
□ Σ+ from VNI with afterburning
dN/dY
Y of Σ+
0
2
4
6
8
10
12
14
0
1
2
3
4
5
6